Phytoplankton detection study through hyperspectral signal in Patagonian Fjords

Pilar Aparicio-Rizzo[1, 2], Dagoberto Poblete-Caballero[1], Cristian Vera-Bastidas[1], Iván Pérez-Santos[1] and Daniel Varela[1]

[1]Centro i~mar, Universidad de Los Lagos, Puerto Montt, Chile
[2]Centro del Clima y la Resiliencia CR2, Santiago de Chile, Chile

Correspondence to: Daniel Varela (dvarela@ulagos.cl); Pilar Aparicio-Rizzo (papariciorizzo@gmail.com)

Abstract. Over recent decades, monitoring coastal areas has becoming a priority due to human population pressure. These areas constitute biodiversity enclaves where the increment in phytoplankton blooms has become a socio-ecological problem with severe impacts at global and regional scales. An important area they affect is the Patagonia ~~F~~fjords, a complex and intricate coastal system strongly exposed to climate forcings and anthropogenic impacts with the aquaculture industry (salmon and mussel farming) as the main source of income. Within this context, fast and accurate monitoring of phytoplankton in the area is crucial. In this study, we focus on using a new technology combining hyperspectral sensors and unmanned aerial vehicles (UAVs) to detect, identify, and differentiate phytoplankton species from optical data. Findings show differences not only between diatoms and dinoflagellates through the shape and magnitude of the spectral signal at 440, 470, 500, 520, 550, 570, and 580 nm but also at the genus level (*Rhizosolenia* sp., *Pseudo-nitzschia* sp., *Skeletonema* sp., *Chaetoceros* sp., and *Leptocylindrus* sp.) and even species level like *Heterocapsa triquetra*. Chlorophyll-a concentration played a key role in reflectance spectra, showing high variability in the green-red bands (~ 500-750 nm) at low concentrations (< 2 µg L^{-1}), and even greater at the blue bands (~ 400-490 nm) under higher concentrations (> 4 µg L^{-1}). Although this work presents a step forward in using new tools and monitoring methodology of phytoplankton in complex coastal systems with a new identification route, more high-quality data from a wide range of ecosystems and environments is still necessary.

1 Introduction

Phytoplankton constitutes an essential group of organisms in aquatic ecosystems. ~~As part of their essential role, t~~They form the base of food webs, are key species in Carbon (C) and Nitrogen (N) biogeochemical cycles, and provide ecosystem services in the ocean (Legendre, 1990**;** Le Quéré et al., 2005). However, phytoplankton can also be harmful to the environment and humans. Intense phytoplankton blooms of several~~many~~ species have multiple negative impacts on coastal systems.~~,~~ These negative effects occur by changing the water quality (e.g., oxygen reduction, turbidity, unpleasant odours) and by the blooms ~~of including the suffocation of marine organisms, negative aesthetic impacts on water quality, murky water sometimes containing floating dead organisms, and the unpleasant odours they produce. These negative impacts have significant~~

~~consequences for local socio-economical activities (Berdalet et al., 2016; León-Muñoz et al., 2018; Díaz et al., 2019; Gobler, 2020). Furthermore,~~ of several ~~phytoplankton~~ species~~, classified as harmful species~~ (~~> 100~~ ~200 known taxa; Hallegraeff et al., 2021)~~ (Sournia, 1995), can~~ that can produce toxins ~~with~~ which enter to the food chain having severe consequences in aquatic systems and even human health (Berdalet et al., 2016; León-Muñoz et al., 2018; Díaz et al., 2019; Gobler, 2020). Moreover, harmful algal bloom (HAB) problems seem to show an apparent global increase (Heisler et al., 2008; Anderson, 2012; Glibert, 2020; Gobler, 2020), or at least a perceived positive trend in HABs, mainly related to the increasing need to exploit marine resources driven by human population growth (Hallegraeff et al., 2021). Thus, the HAB problems, coupled with the expected alteration of phytoplankton communities due to climate change, urge to dispose of permanent monitoring to facilitate the essential tasks of forecasting, management and mitigation.~~, including water pollution and poisoning of marine organisms (shellfish, fish, mammals, birds, etc.), allowing the toxins to enter the food chain, which can ultimately even affect human~~Over recent decades, phytoplankton blooms have caused catastrophic events at both environmental and socio-economical levels worldwide (León-Muñoz et al., 2018; Trainer et al., 2020). An apparent global increase in the frequency and intensity of blooms is thought to be driven by climate change and/or anthropogenic eutrophication (Heisler et al., 2008; Anderson, 2012; Glibert, 2020; Gobler, 2020). Changes in phytoplankton community are also expected due to changes in climate and coastal systems, with consequences for the functioning of the biological carbon pump (Henson et al., 2021). These trends and the predicted demographic growth in coastal areas (Neumann et al., 2015; Merkens et al., 2016) require monitoring phytoplankton blooms to facilitate the essential tasks of forecasting, management and mitigation.~~

~~Traditionally, phytoplankton monitoring has been undertaken by collecting water samples at specific points and analysing those ones in the laboratory. This type of monitoring has several drawbacks, in that it is time consuming, expensive, and labour intensive, making large-scale monitoring over a short period impractical. As a result, the monitoring of phytoplankton by remote sensing using satellites was implemented.~~ Monitoring of phytoplankton in surface waters by satellites has been widely used for decades due to their broad spatial coverage and high temporal resolution (Hu et al., 2005; Shen et al. 2012; Shi et al. 2019; Li et al., 2021)~~. Identification of phytoplankton by remote sensing is mainly based on how the species attributes affect the absorbance/reflectance of the electromagnetic spectrum.~~ The optical properties of phytoplankton, such as pigments concentration (algae colour), size, and morphology, affect the reflectance signal, allowing different groups to be distinguished (Moisan et al., 2017; Shi et al. 2019). ~~Spectral bands located in the blue, green, and red to near-infrared areas of the spectrum can be used to detect algal blooms (Mao et al., 2010; Zhao et al. 2010; Gernez et al., 2023).~~ Differences in the major absorbance and/or reflectance peaks along the spectrum have been related to the colour of the algae, and chlorophyll type and concentration (Mao et al., 2010; Moisan et al., 2017; Gernez et al., 2023). For instance, ~~I~~in the green band (~495-580nm), a peak around 570-580 nm has been associated with Bacillariophyta and Haptophyta (brown algae); meanwhile, Chlorophyta (green algae), known to contain chlorophyll-b, display peaks around 540 nm due to their green colour (Jeffrey and Vesk, 1997; Gitelson et al., 1999; Mao et al., 2010). However, ~~A~~although satellite technology has provided important advances in large-scale phytoplankton monitoring, ~~it has limitations. This technology has been useful for~~ detecting and differentiating between the

main phytoplankton groups and even algal bloomsred tides (Hu et al., 2005; Shen et al., 2012; Gernez et al., 2023). this approach for phytoplankton monitoring has limitations. Even if recent advance in satellites missions use hyperspectral sensors (i.e., Plankton, Aerosol, Cloud, ocean Ecosystem, PACE), these ones have several limitations to reach at phytoplankton community composition level (Shen et al., 2012; Muller-Krager et al., 2018). However, lLimitations inthe spatial and the temporal resolutions, the satellite orbit constraints, restricted the limited surface-to-subsurface signal detectioncapture, and or the restricted a restricted number of reflectance bands are considered the main obstacles to distinguish for the discrimination of the dominant bloom-forming species and the identifyingication of the algae (Shen et al., 2012; Muller-Krager et al., 2018; Schaeffer and Myer, 2020).

Even if recent advance in satellites missions use hyperspectral sensors (i.e., Plankton, Aerosol, Cloud, ocean Ecosystem, PACE), these ones have several limitations to reach at phytoplankton community composition level. The spatial, temporal, and spectral resolutions constitute some of the main factors limiting satellites (Shen et al., 2012; Muller-Krager et al., 2018). Coastal areas are complex waters systems under different types of disturbance and fast changes, being necessary high quality resolutions. In these areas, frequent observations are essential to register detect changes across environmental gradients. Therefore, temporal resolutions of monitoring is needed at days or even hours. Also, at spatial scale factors as the pixel size and the width of the spectral signal are crucial. Several studies propose a minimum of 100 m or even smaller pixels size (~30-50 m) and a width spectral signal from blue to red-near infrared lower than 5 nm, as needed to monitor at coastal areas (Shen et al., 2012; Muller-Krager et al., 2018). Nowadays none satellite sensor have all of these resolutions needed to estimate the phytoplankton community composition, biodiversity and blooms occurrence at coastal ecosystems.

Moreover, phytoplankton monitoring is complex in coastal regions with high environmental heterogeneity at different scales, where more frequent temporal and spatial resolution are necessary to detect rapid changes. For instance, in sub-antarcticpolar coastal areas, like the Patagonian Fjords, satellite information availability is limited for part of the year due to high cloudiness and complex coastal morphology (i.e., fjords and channels). Across this coastal area, there is a two-layer water circulation pattern (Valle-Levinson, 2010; Castillo et al., 2016), consisting of a surface layer fed by continental freshwater (Estuarine Water-EW) from rivers, high rainfall and glacial meltwater, flowing from the continent, and a subsurface layer of salty, nutrient-rich Sub-Antarctic Waters (SAAW) coming from the western Pacific Ocean (Dávila et al., 2002; Pérez-Santos et al., 2014; Linford et al., 2024). This current circulation results in marked vertical and horizontal gradients with significant meridional and zonal changes in temperature, salinity, stratification, and dissolved and suspended matter (Coloured dissolved organic matter CDOM & Total suspended matter TSM) (Silva and Vargas, 2014; Torres et al., 2014; González et al., 2019; Saldías et al., 2019; Linford et al., 2024). Consequently, this current circulation promote an environmental variability that highly influences phytoplankton distribution, and abundance, and Harmful Algal Blooms (HAB) occurrence (Alves-de-Souza et al., 2008; Jacob et al., 2014; León-Muñoz et al., 2018; Cuevas et al., 2019). At local scales, physical processes like stratification, trigger by both river discharge and seasonal solar heating, and biogeochemical water characteristics, including dissolved and suspended matter (CDOM and TSM) and phytoplankton concentration, significantly influence the water's

~~optical properties (Simis et al., 2017; Adhikari et al., 2023)~~. ~~Thus,~~C~~coastal and estuarine waters are considered optically complex due to their high charge and temporal (from daily to seasonal) variability in both biological (phytoplankton) and non-biological (CDOM & TSM) suspended particles that impact directly at the optical signal affecting the water transmission of irradiance (Simis et al., 2017; Adhikari et al., 2023).~~

The accurate observation of phytoplankton in coastal areas where phytoplankton population characteristics can change rapidly over short time scales (hours to days) and at small spatial scales (< 100 m) represents a significant challenge. This observation is important in the Patagonian Fjords, which hosts one of the largest aquaculture industries globally (salmon and shellfish). These industrial activities have suffered recurrent ~~Harmful Algal Blooms (~~HAB~~)~~, experiencing significant damage over recent decades (León-Muñoz et al., 2018; Díaz et al., 2019), with remarkable social, economic and ecosystemic impacts (Soto et al., 2019; Ugarte et al., 2022). Thus, developing and implementing an effective phytoplankton monitoring regime with high accuracy and resolution is essential. However, ~~this~~ implement an effective monitoring has been a tough task due to the complexity and unknown aspects of phytoplankton bloom dynamics.~~,~~ Factors such as ~~together with~~ the broad species diversity involved, ~~and~~ the complex topography and the climate ~~(cloudy hyper-humid)~~ heterogeneity (cloudy hyper-humid) in the study area ~~which~~ directly affect monitoring capacity (Garreaud et al., 2013).

~~Monitoring at t~~The required spatial and temporal resolution can now be achieved through~~due to~~ advances in technology, including unmanned aerial vehicles (UAVs) equipped with sensitive instruments, which have recently become more widely used as platforms in marine monitoring (Kislik et al., 2018; Kimura et al., 2019; McEliece et al., 2020; Hong et al., 2021). Specifically, the use of ~~multi- and~~ hyperspectral cameras that capture in situ reflectance signals at low altitudes (< 100 m) through the visible to near-infrared regions of the spectrum (~ 400-1000 nm) out-performing multispectral cameras and satellites (Moses et al., 2012; Olivetti et al., 2023). Identification of phytoplankton species by hyperspectral images provides a new tool for monitoring in situ the temporal and spatial variation at the local scale in coastal complex ecosystems ~~at high temporal resolutions of days or even hours~~. This optical technology has potential for monitoring phytoplankton and detecting HAB in coastal environments due to its continuous spectrum, with more than 160 values from blue to red bands (400-750 nm), under a low width spectral signal of 2 nm in contrast to a width signal of 10 or even 23 nm used in other sensors, which allow for an accurate phytoplankton characterisation through reflectance (Shen et al., 2012; Van der Merwe and Price, 2015; Wu et al., 2019; Olivetti et al., 2023). Recent studies have illustrated the usefulness of this technology for detecting phytoplankton blooms through the accumulations of algae (Szekielda et al., 2007), the differences in reflectance spectra between recurrent and non-recurrent blooms areas with changes in the green (~ 545-575 nm) and red bands (~ 650-700 nm), respectively (Min et al., 2021), and even the capacity of hyperspectral reflectance data to estimate phytoplankton through pigments concentrations changes, not just the main phytoplankton pigment chlorophyll as satellites, but also secondary pigments as phycocyanins (Shen et al., 2012).

In the present study, we explore the advantages and disadvantages that a hyperspectral camera, coupled with a UAV, offers in detecting phytoplankton from reflectance (R(λ)) at complex coastal waters in remote areas. The main objective was the

characterisation of the reflectance spectra of different phytoplankton assemblages, either harmful or non-harmful, dominated by a single species. By analysing differences in the magnitude and shape at the spectral signal, we seek to distinguish distinct phytoplankton groups.

2 Materials and methods

2.1 Study area

The study area is located within one of the 3 main fjords' regions worldwide at north Patagonia (~ 41.45-42.75° S) in southern Chile (Fig. 1), where most of the national aquaculture activities (salmon, blue mussels, and macroalgae) are found (> 90 %) (Soto et al., 2019).

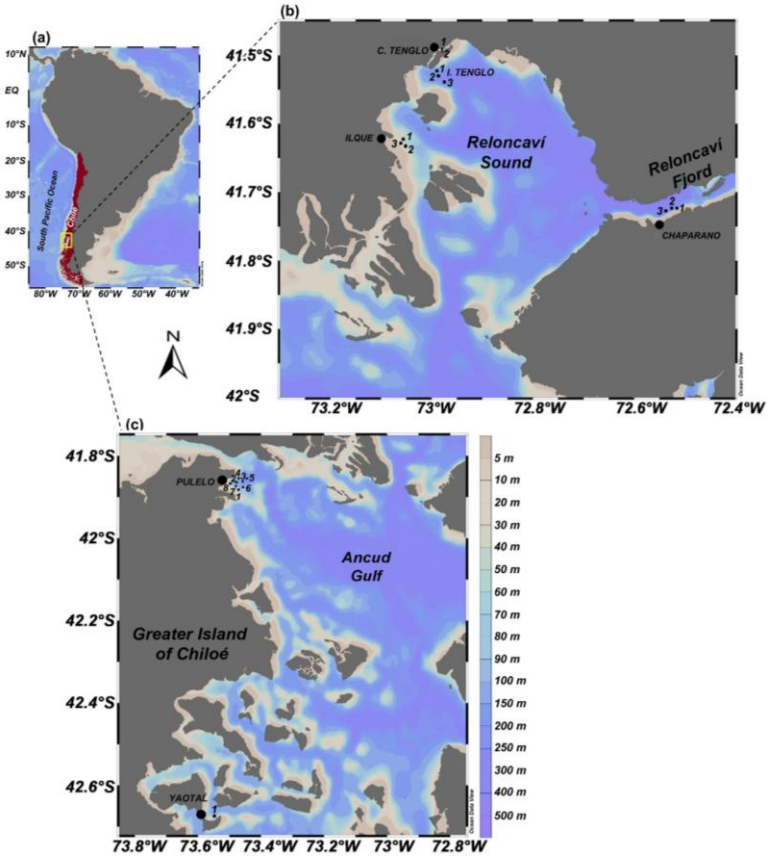

Figure 1: (a) Study area in the Chilean northern Patagonian Fjords (~ 41.45-42.75° S) (yellow), and sampling locations at (b) Reloncaví Sound and (c) Greater Island of Chiloé.

Across this complex coastal system, freshwater inputs from rivers, rain~~precipitation~~, groundwater, and glacial melting generate an estuarine circulation pattern (Dávila et al., 2002; Valle-Levinson, 2010; Castillo et al., 2016), with considerable influence over biogeochemical processes and physical oceanography. The freshwater inputs generate stratification conditions which

strongly influence on bio-optical water properties and support a diatoms-dominated phytoplankton community (Iriarte et al., 2007; Silva et al., 2011; González et al., 2019).

2.2 Field sampling

This study implemented a field sampling strategy from January to May 2023 (austral summer-autumn) in the coastal system to acquire in situ hyperspectral images and oceanographic data for temperature, salinity, and phytoplankton.
Specific sectors were selected for the in situ sampling across the study area (Fig. 1) based on a set of criteria including historical physical-chemical characteristics (temperature, salinity, and turbidity), local circulation, HAB occurrence, and proximity to aquaculture installations (Table S1) (Silva et al., 2011; Soto et al., 2019; Soto et al., 2021).

Table S1: Characteristics of in situ sampling sectors.

Location	Stations	Date (dd/mm/yyyy)	Latitude	Longitude	Sechii Depth (m)	Characteristics and criteria for selecting the sampling area
Ilque (I)	I1	05/01/2023	-41.621	-73.063	5.01	Semi-enclosed circulation area Clear-Turbid waters Strong marine influence HAB moderate risk
	I2	05/01/2023	-41.630	-73.059	4.57	
	I3	31/03/2023	-41.627	-73.064	10.25	
Pulelo (P)	P1	18/01/2023	-41.873	-73.477	3.68	Intense salmon culture activity Open circulation area Clear waters Strong marine influence HAB medium risk
	P2	18/01/2023	-41.864	-73.480	4	
	P3	18/01/2023	-41.861	-73.467	4.38	
	P4	18/01/2023	-41.855	-73.476	5.22	
	P5	08/03/2023	-41.856	-73.459	12.31	
	P6	08/03/2023	-41.868	-73.467	10.59	
	P7	08/03/2023	-41.868	-73.482	7.43	
	P8	08/03/2023	-41.865	-73.498	8.15	
Isla Tenglo (I)	T1	26/01/2023	-41.524	-72.991	3.74	Open circulation area Clear waters Strong marine influence HAB moderate risk
	T2	26/01/2023	-41.531	-72.987	4.05	
	T3	26/01/2023	-41.539	-72.969	4.325	
Yaotal (Y)	Y1	12/04/2023	-42.672	-73.548	13.08	Intense salmon culture activity Open circulation area Clear waters Strong marine influence HAB medium risk
~~C.~~ Chaparano (C)	C1	14/04/2023	-41.724	-72.520	4.48	Intense mussel farm activity Enclosed circulation area Turbid waters Freshwater influence HAB high risk Historical HAB occurrence
	C2	14/04/2023	-41.725	-72.527	4	
	C3	14/04/2023	-41.727	-72.536	4.73	
Canal Tenglo (CT)	CT1	09/05/2023	-41.495	-72.984	4.16	Enclosed circulation area Turbid waters Marine influence HAB moderate risk
	CT2	09/05/2023	-41.499	-72.984	4.68	

Six locations were defined across the area using these criteria: Ilque (I), Isla Tenglo (T), and Canal Tenglo (CT) within the Reloncaví sound coastal system, ~~Caleta~~ Chaparano (C) in Reloncaví fjord, and two sampling points along the coast of the Greater Island of Chiloé, Pulelo (P) and Yaotal (Y) (Table S1, Fig. 1b & c). At these monitoring locations, sampling transects of 3 or 4 stations were carried out depending on topography and UAV flight autonomy.

The field sampling was carried out during daylight (~ 10.30-16.00 h local time) under safe and optimal weather conditions. Although meteorological conditions varied between sunny and cloudy days, all sampling transects were conducted under conditions of no rain, low wind speed (< 15 m s^{-1}), and calm surface waters (waves < 1 m).

Water samples for oceanographic monitoring were collected simultaneously with the optical data at each station. The geo-location (latitude/longitude) was sent from the vessel equipment to the UAV technician on shore to coordinate the water sampling with the aerial observations. The autonomous flights were configured using the DJI Pilot 2 drone software for an altitude of 100 m above the sea surface and a flight speed of ~ 1-2 m s^{-1} according to in situ solar radiation to obtain images of an area of 2500 m^2 around the oceanographic sampling points.

As phytoplankton is commonly distributed within the first ~ 20-30 m of the water column, two sampling depths were established: the first at the surface (~ 1.5 m) and the second based on water transparency. Temperature, salinity and in situ Chlorophyll-a (Chl-a) were determined using two CTDs, a RBRconcerto³ and an AML-Oceanographic Metrec XL. On the other hand, transparency was determined by a Secchi disk. Water samples were collected using a Niskin bottle, at the surface and Secchi depths, and stored in opaque plastic bottles to be analysed at the laboratory for both phytoplankton in situ total biomass (Chl-a) and phytoplankton abundance and taxonomy. Discrete water samples collected for analyses of phytoplankton abundance and taxonomy were fixed with Lugol's iodine solution (1 %).

Con formato: Fuente: Sin Cursiva

Con formato: Fuente: Sin Cursiva

2.3 Phytoplankton analysis

Phytoplankton species abundance was estimated in the microphytoplankton range (~ 20-200 µm) at the laboratory. The phytoplankton identification and cell counts were made following Utermöhl method (Utermöhl, 1958), i.e. 10 mL of fixed water sample was settled from day to day and then observed using an inverted light microscope (Olympus CKX-41). Taxonomic identification was made to the lowest level possible (genus or species) (Mardones and Clément, 2016; Lincoqueo, 2019).

2.4 UAV system, reflectance measurement and hyperspectral image

The UAV used in this study was a DJI Matrice 300 RTK drone with the capacity to support a maximum weight of ~ 9 kg and a flight autonomy of approximately 30 minutes (Fig. 2a). A hyperspectral camera Resonon Pika L model was coupled to the drone by a custom made 3D printed carbon fibre gimbal (Fig. 2b). In addition, a minicomputer Intel NUC was carried by the drone attached using a custom 3D printed mount, including batteries (Fig. 2b).

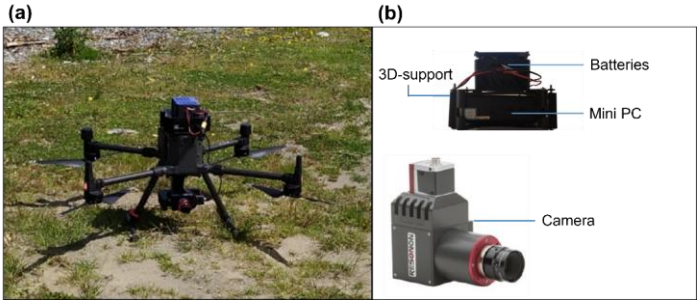

Figure 2: UAV system: (a) DJI Matrice 300 RTK drone, and (b) Resonon Pika L hyperspectral camera, and the 3D printed mount with the batteries and minicomputer Intel NUC.

The camera captures 236 spectral bands covering a spectrum range from ~ 400 to 900 nm with a spectral resolution of approximately ~ 2.1 nm. A Flame S spectrometer (Flame Ocean Insight) was used for recording the light conditions (solar radiation) during the flight in the same spectral bands as those captured by the hyperspectral camera.

A laptop connected via a cellular connection or a Wireless Local Area Network (WLAN) ~~network~~ to the minicomputer was used to operate the camera and record reflectance data. In remote areas where connectivity was not available, communication between computers was established by an Access Point Ubiquiti Loco M5 through a local wireless network.

2.5 Data processing and analyses

Before the data analyses, a pre-selection was performed, removing all the samples with several co-occurring phytoplankton genera (> 3) from the final dataset. Only stations where one or a maximum of two genera dominated the community by > 80 % of abundance were considered for the reflectance fingerprint analysis and the differentiation among the spectral signals.

Several steps were involved in processing the raw image data captured by the hyperspectral camera using the Spectronon Pro software. The raw data were processed to obtain reflectance (R(λ)) using the calibration file provided by Resonon and the downwelling irradiance data provided by a miniature spectrometer (Flame Ocean Insight). Next a pixel cleaning by an adapted Normalized Difference Water Index (NDWI) ~~index~~ was undertaken, masking those pixels that did not correspond to water and those saturated due to solar radiation angle incidence (Xie et al., 2014). Due to the lack of reference points in the monitoring areas non geometric correction was applied to the raw image data. Because of this the raw data were used only as reflectance data instead of images in this study. These data were normalized using the min-max method. After that, the Savitzky-Golay method or digital smoothing polynomial filtering (DISPO), based on least squares polynomial smoothing fit and differentiation (Ruffin and King, 1999; Gallagher, 2020), was applied to reduce the signal of the noise and obtain a clean spectrum without

altering its properties. Finally, reflectance raw data were averaged, obtaining a reflectance value at each band to emphasise the shape singularities of each spectrum.

For analysing and comparing the spectral signals of the different phytoplankton species, the reflectance R(λ) values were used at a spectral resolution of ~ 2.1 nm approx., and the wavelength bands were limited to the visible and near-infrared light between 400 and 750 nm.

A hierarchical cluster analysis (HCA) was made to explore the changes in R(λ) under different genera domains. A resemblance matrix based on the hyperspectral normalised R(λ) was generated using the nearest neighbour single linkage algorithm and the cosine index as a distance measure for calculating the similarity among spectral signals.

Differentiation among spectral signals for the stations under the same phytoplankton genus domain was analysed using the non-parametric Kolmogorov-Smirnov test. In addition, to assess the influence of pigment concentration at spectral signals, a statistical analysis was applied to determine the differences among low (< 2 µg L^{-1}), moderate (> 4 µg L^{-1}) and high (> 8 µg L^{-1}) Chl-a concentrations.

Con formato: Fuente: Sin Cursiva

The in situ temperature and salinity were converted to the conservative temperature and absolute salinity by applying the algorithms proposed in the Thermodynamic Equation of Seawater 2010 (TEOS-10). The conservative temperature is similar to potential temperature, but represents the heat content of seawater with more precision. Absolute salinity, on the other hand, represents the spatial variation in the composition of seawater, taking into account the different thermodynamic properties and the horizontal density gradient in the open ocean (IOC et al., 2010).

Oceanographic variables across the study area were characterised at a seasonal scale ~~and in depth using a principal component analysis (PCA) to produce an ordination of sampling stations~~, with~~followed by~~ a permutational analysis of variance (One-way PERMANOVA) to determine the differences between stations. Before the analysis, data were homogenised (log-transformed) and normalised to better approximate multivariate normality.

Data were visualised and processed using Ocean Data View (ODV) (Schlitzer, 2023), which applied DIVA gridding interpolation (Troupin et al., 2012), PRIMER 7 (Clarke and Gorley, 2015), and PAST 4.06 softwares (Hammer et al., 2001).

3 Results

~~3.1 Oceanographic Conditions~~

~~The temperature profiles generally displayed surface warming, especially in summer, with a clear development of thermal stratification conditions (Fig. 3a).~~

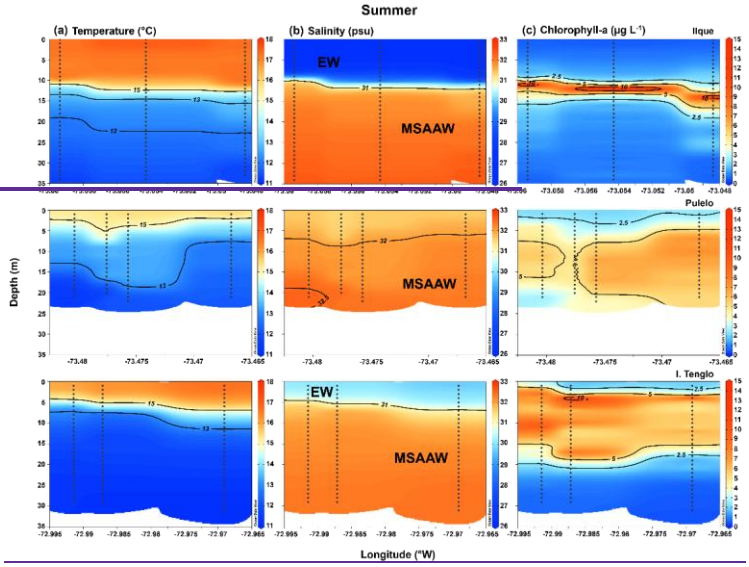

Figure 3: Oceanographic conditions of (a) Temperature, (b) Salinity, and (c) Chlorophyll-a at the sampling locations during summer. EW (Estuarine Water), MSAAW (Modified Sub-Antarctic Water).

Temperatures in the autumn were generally lower (a difference of ± 2.2-5.7° C) with weaker depth gradients, except of Chaparano in the Reloncaví fjord (Fig. 4a).

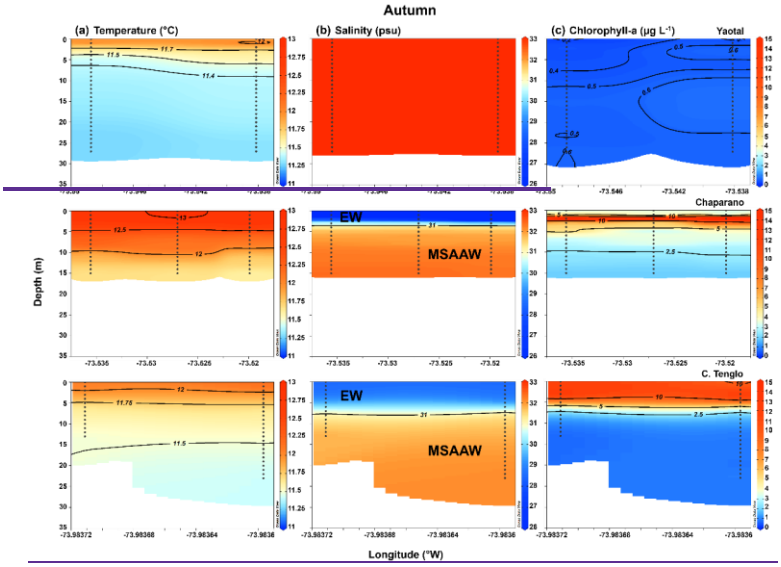

~~**Figure 4: Oceanographic conditions of (a) Temperature, (b) Salinity, and (c) Chlorophyll-a at the sampling locations during autumn. EW (Estuarine Water), MSAAW (Modified Sub-Antarctic Water).**~~

~~Freshwater input clearly influenced the salinity observed around the Reloncaví sound and within the fjord (Fig. 3b and 4b), with the lowest salinity values at Chaparano (Table 2). On the other hand, an influence of oceanic water was detected, with the highest salinity, at Greater Island of Chiloé, where estuarine water (EW) was not detected (Fig. 3b and 4b).~~

~~**Table 2: Oceanographic conditions of Temperature (T), Salinity (S), and Chlorophyll-a (Chl-a) at the sampling locations. Mean, Standard deviation (SD) and Range (maximum-minimum).**~~

~~Sampling Location~~	~~Station~~	~~Date~~	~~Mean T±SD (°C)~~	~~Mean S±SD~~	~~Mean Chl-a±SD (µg L⁻¹)~~	~~Range T (max. min.) (°C)~~	~~Range S (max. min.)~~	~~Range Chl-a (max. min.) (µg L⁻¹)~~
~~Ilque~~	~~I1/I2~~	~~05/01/2023~~	~~17.34±0.17~~	~~26.98±0.08~~	~~0.80±0.35~~	~~17.48 17.12~~	~~27.07 26.88~~	~~1.04 0.55~~
~~Pulelo~~	~~P1/P2/P3/P4~~	~~18/01/2023~~	~~14.94±0.60~~	~~31.69±0.16~~	~~2.92±1.01~~	~~14.02 15.51~~	~~31.91 31.48~~	~~4.79 2.02~~
~~Isla Tenglo~~	~~T1/T2/T3~~	~~26/01/2023~~	~~16.00±0.49~~	~~30.16±0.35~~	~~5.93±4.51~~	~~15.22 16.64~~	~~30.70 29.69~~	~~12.21 1.58~~
~~Ilque~~	~~I3~~	~~31/03/2023~~	~~12.36±0.25~~	~~31.96±0.03~~	~~1.55±0.82~~	~~12.18 12.54~~	~~31.93 31.98~~	~~0.97 2.13~~
~~Yaotal~~	~~Y1~~	~~12/04/2023~~	~~11.66±0.45~~	~~33.29±0.01~~	~~0.44±0.16~~	~~11.35 11.98~~	~~33.28 33.30~~	~~0.33 0.56~~
~~Chaparano~~	~~C1/C2/C3~~	~~14/04/2023~~	~~12.76±0.20~~	~~26.39±5.69~~	~~4.58±1.14~~	~~13.01 12.47~~	~~31.73 20.05~~	~~6.10 3.21~~

Canal Tenglo	CT1/CT2	09/05/2023	11.99±0.20	28.79±0.28	10.16±1.41	12.21-11.79	29.07-28.55	11.47-8.54

In the summer, Chl-a concentrations were highest around the transitional depth between the estuarine and modified sub-Antarctic water masses (Fig. 3c). Meanwhile, in autumn, the highest values were detected in the low salinity surface waters (EW) (Fig. 4c), with a minimum in Chl-a at Yaotal under a homogeneous water column (Fig. 4c, Table 2) and the maximum at Canal Tenglo associated with a phytoplankton bloom event (Fig. 4c). Across the sampling locations, the highest values (> 4 $\mu g\ L^{-1}$) and largest ranges were observed in enclosed waters, i.e., Chaparano and both Canal Tenglo and Isla Tenglo (Fig. 1b, Table 2).

The analysis of the oceanographic variables' spatial patterns (temperature, salinity, and Chl-a) indicates that 74 % of oceanographic variability is explained by the first two components (Fig. 5). For the first component (PC1), the highest eigenvector was exhibited by Chl-a (- 0.67) followed by temperature (0.62), with both variables significantly associated with PC1 scores ($p < 0.01$). Meanwhile, salinity was significantly correlated with PC2 scores ($p < 0.01$), with the relevant eigenvector (- 0.89) in the second component (PC2).

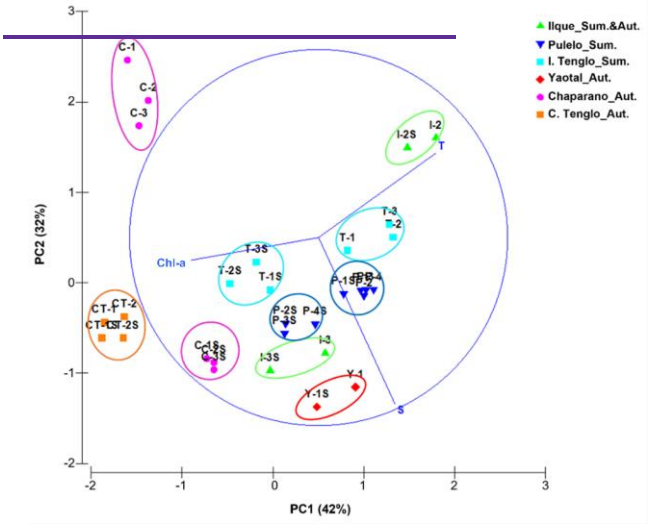

Figure 5: Spatial ordination diagram of sampling locations based on oceanographic conditions (blue vectors T, S, Chl-a) at Surface and Secchi depths (S), observed during Summer (Sum.) and Autumn (Aut.). T= temperature, S= salinity, and Chl-a= chlorophyll-a.

~~This analysis indicates that the summer samples at Ilque (I-2), Pulelo (P) and Isla Tenglo (T) were mainly influenced by temperature and Chl-a (Fig. 5). Whereas autumn samples were influenced by Chl-a and salinity (Fig. 5). Chaparano (C) and Canal Tenglo (CT) were mainly influenced by Chl-a, but Yaotal (Y) and Ilque (I-3) by salinity (Fig. 5).~~

~~Significant differences in oceanographic conditions were registered between seasons ($F = 8.18$, $p < 0.01$), but not between depths ($F = 2.2$, $p > 0.05$). However, in summer, differences were observed in Chl-a and temperature between surface and Secchi depth at both Pulelo and Isla Tenglo (Fig. 5). While, in autumn, there was a pronounced difference in salinity with depth at Chaparano (Fig. 5).~~

3.12 Phytoplankton and spectral signals

Con formato: Diseño: Claro (Anaranjado claro)

Although the phytoplankton community was typical of the summer-autumn diatoms assemblage described for the area, the community composition changed between seasons, with an increase in diversity and a decrease in dominance together with a slight increase in richness in the autumn, except for Canal Tenglo (Fig. 36, Table S24).

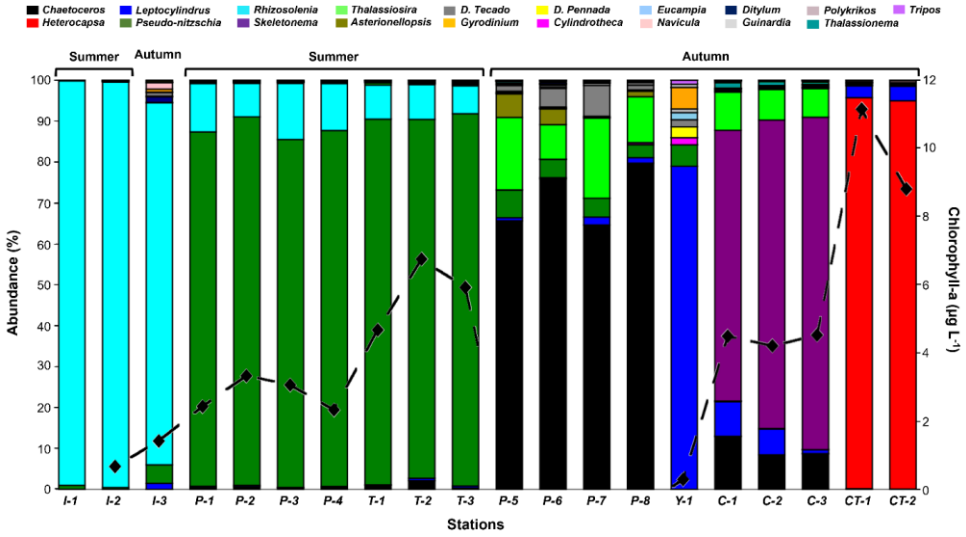

Figure 36: Microphytoplankton community composition (histogram) and total biomass (black line) during summer and autumn at sampling localities~~locations~~. Each colour represents a genus of the community. Code localities~~locations~~: I= Ilque, P= Pulelo, T= Isla Tenglo, Y= Yaotal, C= Chaparano, and CT= Canal Tenglo.

Even though only a bloom of microalgae *Heterocapsa triquetra* was detected during the study period, composition analysis showed a clear mono-genus domain (> 80 % abundance) of *Rhizosolenia* sp. at Ilque, and *Pseudo-nitzschia* sp. at Pulelo and Isla Tenglo in the summer (Fig. 3~~6~~). On the other hand, in autumn a combination of two genera was needed to reach 80 % abundance at Chaparano, Yaotal and Pulelo (Fig. 3~~6~~).

Although the reflectance spectrums, under a diatom genus domain, displayed quite similar patterns across the blue and green bands (~ 400-565 nm), differences in the shape of the curve and the reflectance values were observed, even between sample stations at the same location (Fig. 4~~7~~ and 5~~8~~). During summer, samples at Ilque, dominated by *Rhizosolenia* sp., displayed significant differences in the spectral signal ($p < 0.01$) between stations in both the blue (~ 400-490 nm) and green to near infra-red ~~bands~~ (~ 500-750 nm) bands (Figure 4~~7~~a, Table S3~~2~~).

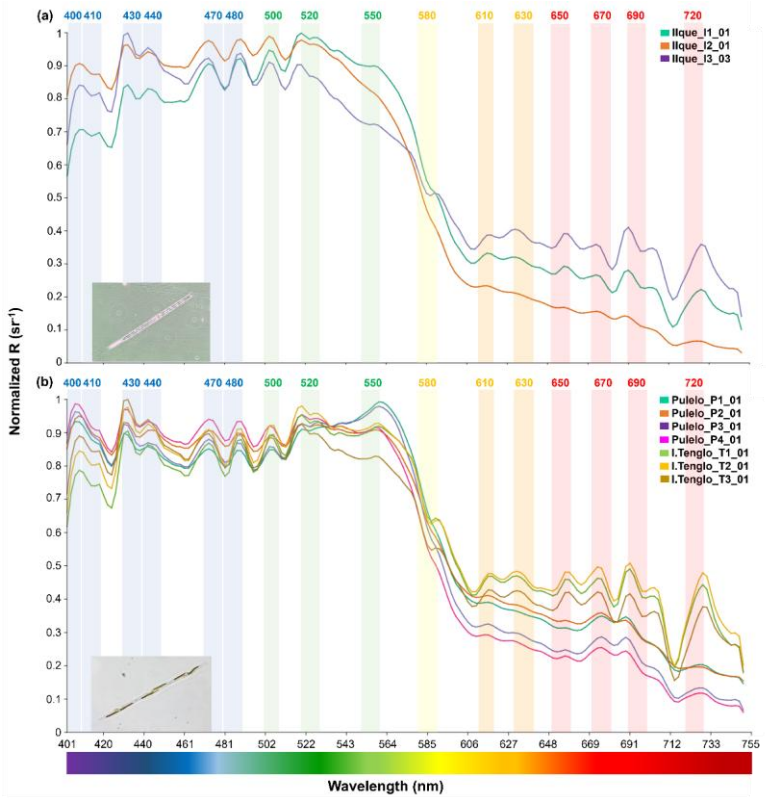

Figure 4~~7~~: Diatoms spectral signals: (a) *Rhizosolenia* sp. at Ilque (aqua green, orange and purple), and (b) *Pseudo-nitzschia* sp. at Pulelo (aqua green, orange, purple and pink) and Isla Tenglo (jasmine green, yellow and brown) in north Patagonia (~ 41.45°-42.75° S).

Similarly, under *Pseudo-nitzschia* sp. domain, significant spectral differences ($p < 0.01$) were detected at Pulelo in the total spectrum (Table S3~~2~~). In the blue ~~bands~~ (~ 400-490 nm) bands, similar signals at stations 1 and 3 differ from stations 2 and 4 (Fig. 4~~7~~b, Table S3~~2~~). Meanwhile, from green to the near infra-red ~~bands~~ (~ 500-750 nm) bands, stations 1 and 2 differed significantly in the spectral signal at stations 3 and 4 (Fig. 4~~7~~b, Table S3~~2~~). On the other hand, at Isla Tenglo, only station 3 displayed a spectral signal significantly different in the green to the near infra-red ~~bands~~ (~ 500-750 nm) bands (Fig. 4~~7~~b, Table S3~~2~~).

Generally, tThe analysis displayed a more homogeneous reflectance signal from March to April (autumn) samples (Fig. 58). At Pulelo, similar spectral signals were detected, except for station 8 (Fig. 58a, pink), in the green to the near infra-red bands (~ 500-750 nm) bands (Fig. 58a, Table S32). Also, only station 2 at Chaparano (Fig. 58b, orange) displayed a statistically different total spectrum ($p < 0.05$) and spectral signal in the blue band (~ 400-490 nm) bands ($p < 0.01$) (Fig. 58b, Table S32).

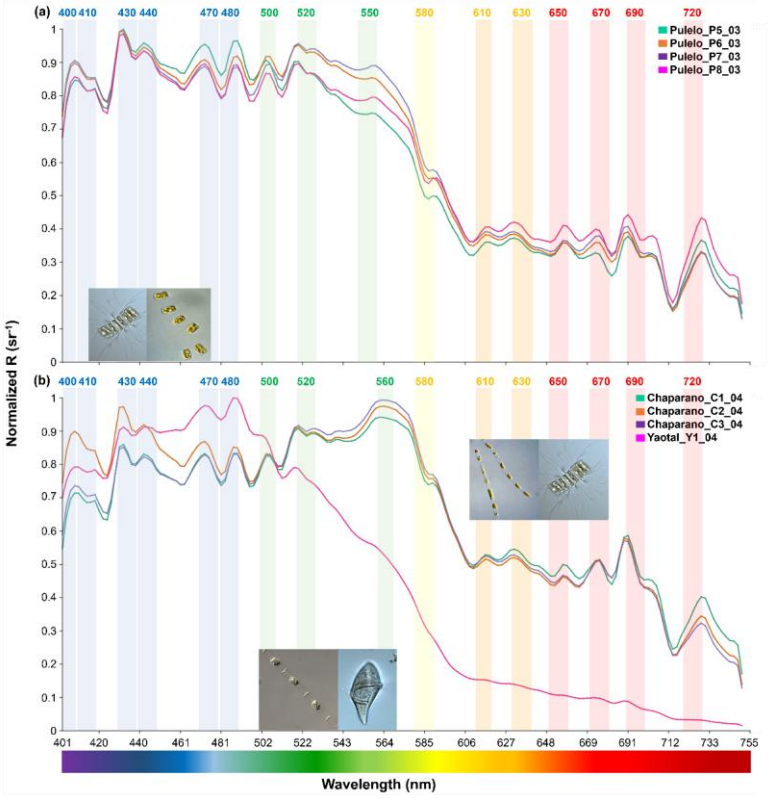

Figure 58: Diatoms spectral signals: (a) *Chaetoceros* sp. & *Thalassiosira* sp. at Pulelo (aqua green, orange, purple and pink), and (b) *Skeletonema* sp. & *Chaetoceros* sp. at Chaparano (aqua green, orange and purple), and *Leptocylindrus* sp. & *Gyrodinium* sp. at Yaotal (pink) in north Patagonia (~ 41.45°-42.75° S).

A comparison between the bands indicated that all samples under diatoms genera domain displayed a similar pattern in the blue bands (~ 400-490 nm) bands, except for *Leptocylindrus* sp. at Yaotal, with the highest R(λ) (> 0.9 sr^{-1}) registered at 470-

480 nm (Fig. 58b). In the green bands (~ 500-565 nm) bands, where chlorophyll pigments reflect light, generally high values of reflectance (> 0.9 sr^{-1}) were recorded, but also a higher variability in both shape and R(λ) values (Fig. 47 and 58). In fact, at Ilque, where *Rhizosolenia* sp. dominated, the reflectance exhibited an acute downward slope between the green and yellow bands (~ 550-610 nm) bands (Fig. 47a), where the absorption peaks of accessory pigments such as phycoerythrin and phycocyanin are usually detected. A similar slope was observed at Pulelo and Isla Tenglo under *Pseudo-nitzschia* sp. domain (Fig. 47b). While, at Chaparano, this slope was less pronounced (Fig. 58b).

Finally, the spectral reflectance from all diatom genera displayed a declining slope in the red to near-infra-red bands (~ 650-740 nm) bands, where another peak in chlorophyll reflectance is typically described. In this area of the spectrum, two main peaks were observed between ~ 680-720 nm and an acute decline at ~ 714 nm (Fig. 47 and 58). A Strong variability was registered among genera in this area of the spectrum, with the highest values detected at Chaparano for the *Skeletonema* sp. and *Chaetoceros* sp. assemblage (Fig. 58b).

Furthermore, important differences were observed in the spectra between diatoms and dinoflagellates. The spectral signal of dinoflagellates was captured only once, under a bloom of the species *Heterocapsa triquetra*. The spectrum shape of this species displayed a completely different pattern compared to those of diatom genera. In the *Heterocapsa triquetra* spectral signal, a clear increase in the R(λ) from the blue to green bands (~ 400-565 nm) can be observed (Fig. 69).

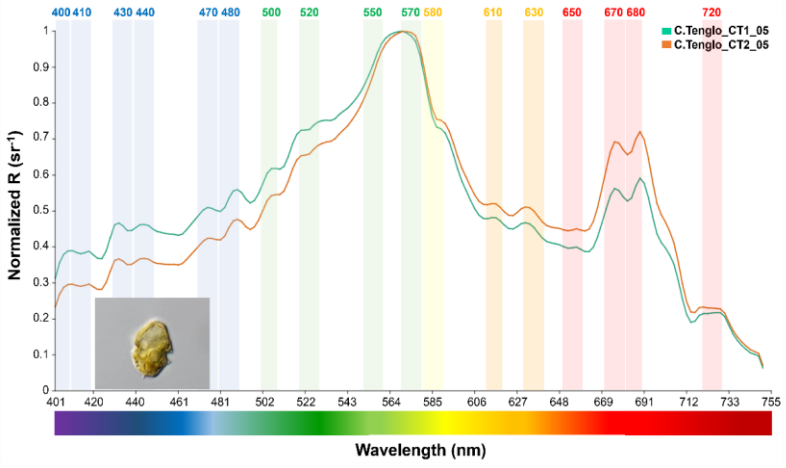

Figure 69: Dinoflagellate *Heterocapsa triquetra* spectral signal at Canal Tenglo (aqua green-Sta.1, orange-Sta.2) in north Patagonia (~ 41.45°-44.75° S).

R(λ) values were two or three times lower than for diatoms in the blue bands (~ 400-490 nm) bands (Fig. 4, 5 and 6), with differences between station signals (Table S3) (Fig. 47, 58 and 69). The main peak of R(λ) was at 570 nm in the yellow-green

area (Fig. 6~~9~~). Differences between dinoflagellates and diatoms were also registered in the red to near infra-red ~~bands~~ (~ 650-740 nm) bands with a distinctive signal of two R(λ) peaks at 670 and 680 nm (> 0.55 sr^{-1}), together with a plateau structure at 720 nm (Fig. 4~~7~~, 5~~8~~ and 6~~9~~).

In summary, differences between groups were detected through the shape (Fig. 4~~7~~, 5~~8~~ and 6~~9~~), the peaks observed at 440, 470, 500, 520, 550, 570, and 580 nm, and the variations in the magnitude displayed in the blue-green (~ 400-565 nm) and red to near infra-red ~~bands~~ (~ 650-740 nm) bands (Fig. 4~~7~~, 5~~8~~ and 6~~9~~). ~~As a result, the cluster analysis grouped spectra corresponding to stations under the same dominant groups and genera closer (Fig. 710).~~

3.2 Oceanographic condition and their relation with the reflectance

Oceanographic conditions denoted seasonal differences ($F= 8.18$, $p < 0.01$), where the highest conservative temperature was registered in summer 2023, ranging from 14°-18° C (Fig. 7a, b). In autumn, the water temperature has reduced the variability, and maximum values did not exceed 13° C in the surface layer (Fig. 7c, d).

Con formato: Fuente: Negrita

Con formato: Espacio Antes: 0 pto, Después: 0 pto

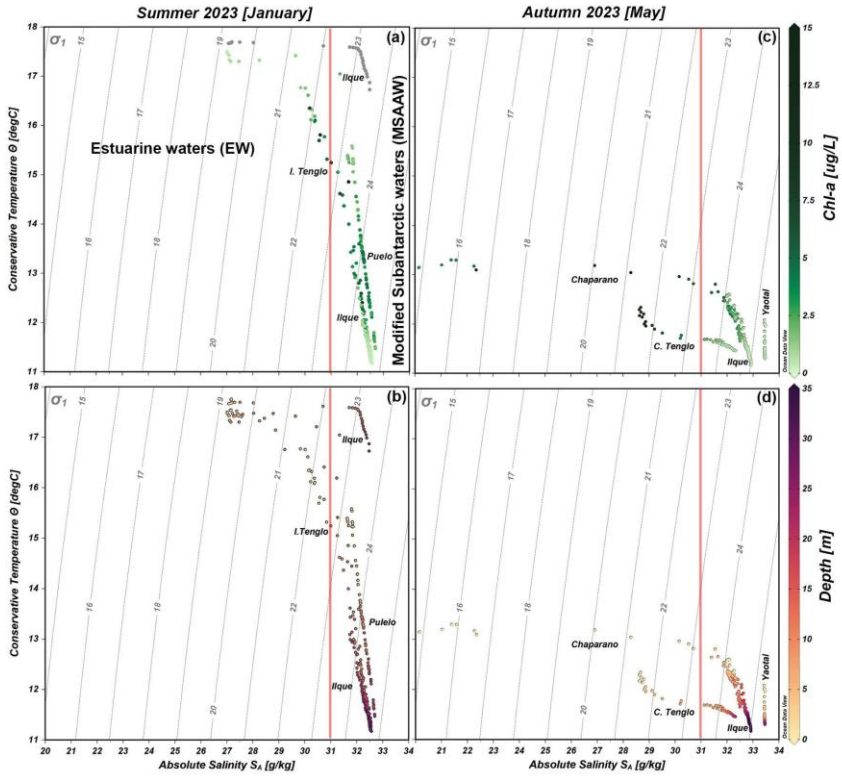

Figure 7: Conservative temperature and absolute salinity scatter diagram, including the density (σ) isoline (grey vertical lines) collected during the 2023 summer and autumn oceanographic campaigns. (a and c) Incorporated the Cehl-a, and (b and d) the depth where the data was obtained. In (a) the grey dot in the Ilque area denoted no Chl-a data.

Con formato: Fuente: 9 pto, Negrita

~~Oceanographic conditions denoted seasonal differences (F= 8.18, p < 0.01), where the highest conservative temperature was registered in summer 2023, ranging from 14°-18° C (Figure 7a, b). In autumn, the water temperature has reduced the variability, and maximum values did not exceed 13° C in the surface layer.~~ Moreover, the absolute salinity minimum was observed during the autumn in the surface layer (20-22 g/kg) of Chaparano, contributing with the decrease in the water density (Fig.~~ure~~ 7d), while in summer, absolute salinity varied from 26-33 g/kg (Fig.~~ure~~ 7b~~e~~). According to the salinity criteria (Silva et al., 2008),

Estuarine Water (0-31 g/kg) and Modified Subantarctic Water (31-33 g/kg) were observed along both seasonal stations. In the case of Chl-a distribution, maximum values (15 µg/L) were registered at the surface layer of the Canal Tenglo during autumn, but in general, no pattern was observed.

However, considering only the chlorophyll-a, the reflectance spectra displayed variability under different Chl-a concentrations (Fig. 8). Significant differences ($p < 0.01$) in spectra signals were detected at Ilque, with *Rhizosolenia* dominant, between January (low Chl-a= 0.8 µg L_a^{-1}) and March (high Chl-a= 1.6 µg L_a^{-1}).

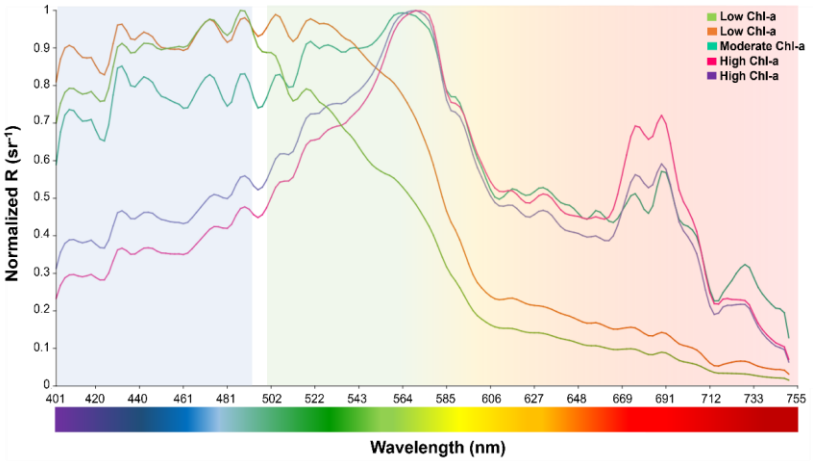

Figure 8: Microphytoplankton spectral signals at different Chlorophyll-a concentration. Low chlorophyll-a (< 2 µg L_a^{-1}) (jasmine, green and orange lines); Moderate chlorophyll-a (> 4 to 7.9 µg L_a^{-1}) (aqua green line); and High chlorophyll-a (> 8 µg L_a^{-1}) (pink and purple lines).

Also, in January, Pulelo (low Chl-a= 2.92 µg L_a^{-1}) and Isla Tenglo (high Chl-a= 5.93 µg L_a^{-1}) exhibited significant differences ($p < 0.01$) with a *Pseudo-nitzschia* dominant.

Regardless of the dominant species, at low Chl-a concentrations (< 2 µg L_a^{-1}), reflectance spectral signals exhibited more significant variability in the green-red bands (from 500 to 750 nm) bands, while under moderate (> 4 µg L_a^{-1}) to high (> 8 µg L_a^{-1}) Chl-a concentrations this variability was greater in the blue bands (~ 400-490 nm) bands (Fig. 8).

Lastly, the cluster analysis grouped spectra corresponding to stations under the same dominant groups and genera closer (Fig. 8). Although similarity values were high, two main divisions were identified: one grouping locations dominated by diatoms and another dominated by the dinoflagellate *Heterocapsa triquetra* (Canal Tenglo) (Fig. 9).

Con formato: Fuente: Cursiva
Con formato: Superíndice
Con formato: Superíndice
Con formato: Resaltar
Con formato: Fuente: 12 pto
Con formato: Fuente: 12 pto
Con formato: Fuente: 9 pto, Negrita
Con formato: Fuente: 9 pto, Negrita, Superíndice
Con formato: Fuente: 9 pto, Negrita
Con formato: Fuente: 9 pto, Negrita, Superíndice
Con formato: Fuente: 9 pto, Negrita
Con formato: Fuente: 9 pto, Negrita, Superíndice
Con formato: Fuente: 9 pto, Negrita
Con formato: Superíndice
Con formato: Superíndice
Con formato: Fuente: Cursiva
Con formato: Superíndice
Con formato: Superíndice
Con formato: Superíndice
Con formato: Espacio Después: 0 pto
Con formato: Fuente: Cursiva
Con formato: Fuente: 10 pto

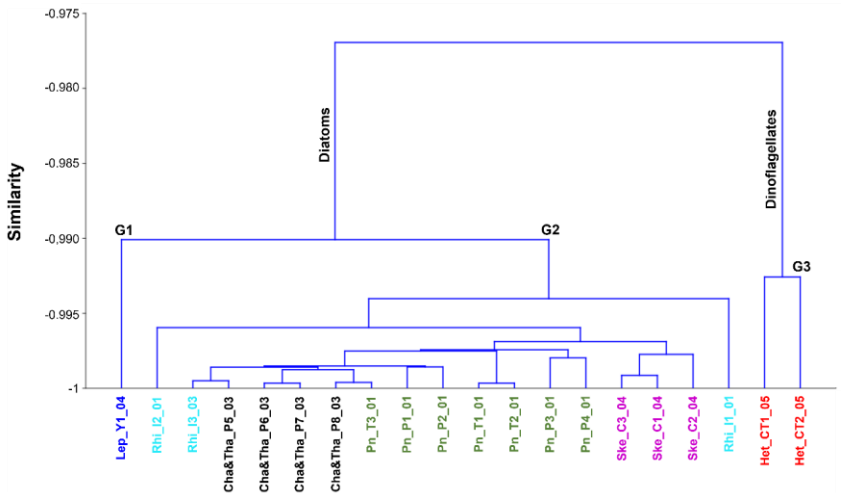

Figure 9871~~0~~: Dendrogram of microphytoplankton hyperspectral normalised R(λ) signals classified by the dominant genus. Colours identify different genus and sampling localities~~locations~~: *Leptocylindrus* sp. in Yaotal (blue), *Rhizosolenia* sp. in Ilque (cyan), *Chaetoceros* sp. & *Thalassiosira* sp. in Pulelo (black), *Pseudo-nitzschia* sp. in Pulelo & Isla Tenglo (green), *Skeletonema* sp. in Chaparano (violet) and *Heterocapsa triquetra* in Canal Tenglo (red).

~~Lastly, Tthe cluster analysis grouped spectra corresponding to stations under the same dominant groups and genera closer (Fig. 8). Although similarity values were high, two main divisions were identified: one grouping locations dominated by diatoms and another dominated by the dinoflagellate *Heterocapsa triquetra* (Canal Tenglo) (Fig. 9871~~0~~).~~

Within the diatoms, 2 groups can be described: a first group (G-1) at Yaotal during the autumn, dominated by *Leptocylindrus* sp. (78.95 %), with the dinoflagellate *Gyrodinium* sp. (5.26 %) as the secondary genus. The second (G-2) grouped the rest of the localities~~locations~~ dominated by diatoms (Fig. 9871~~0~~). Within G-2, all samples were grouped by the dominant genus except Ilque (Fig. 9871~~0~~).

Nevertheless, the dendrogram grouped localities~~locations~~ based on not only the dominant genus but also under similar oceanographic conditions (Fig. 9871~~0~~). Thus, on the left side of the cluster, Yaotal (blue) and Ilque (cyan) were associated with changes in salinity during the autumn season and characterised by low Chl-a values. On the opposite side (right), Canal Tenglo (red) and Chaparano (violet) localities~~locations~~ were characterised by the register of high Chl-a values.

Con formato: Fuente: 10 pto, Sin Negrita

Con formato: Espacio Antes: 12 pto

Con formato: Fuente: Sin Cursiva

Con formato: Fuente: Sin Cursiva

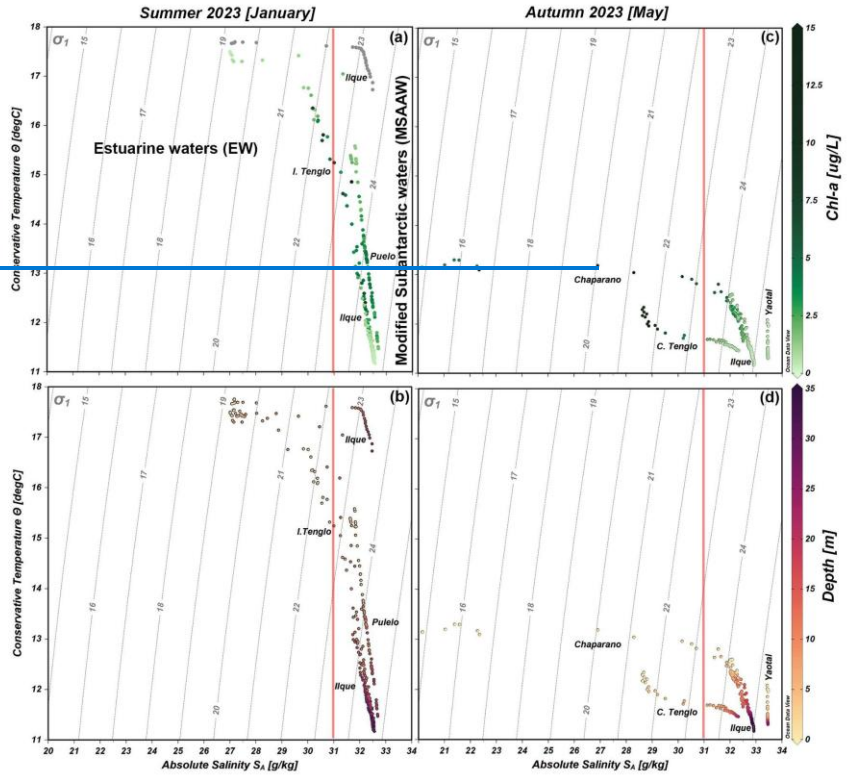

~~Figure 8: Conservative temperature and absolute salinity scatter diagram, including the density (σ) isoline (grey vertical lines) collected during the 2023 summer and autumn oceanographic campaigns. (a and c) Incorporated the chl-a, and (b and d) the depth where the data was obtained. In (a) the grey dot in the Ilque area denoted no Chl-a data.~~

~~Therefore, oceanographic conditions denoted seasonal differences ($F = 8.18$, $p < 0.01$), where the highest conservative temperature was registered in summer 2023, ranging from 14°-18° C (Figure 8a, b). In autumn, the water temperature has reduced the variability, and maximum values did not exceed 13° C in the surface layer. Moreover, the absolute salinity minimum was observed during the autumn in the surface layer (20-22 g/kg) of Chaparano, contributing with the decrease in the water density (Figure 8d), while in summer, absolute salinity varied from 26-33 g/kg (Figure 8c). According to the salinity~~

criteria (Silva et al., 2008), Estuarine Water (0-31 g/kg) and Modified Subantarctic Water (31-33 g/kg) were observed along both seasonal stations. In the case of Chl-a distribution, maximum values (15 µg/L) were registered at the surface layer of the Canal Tenglo during autumn, but in general, no pattern was observed.

HoweverTherefore, reflectance spectra displayed variability under different chlorophyll-a concentrations (Fig. 911).

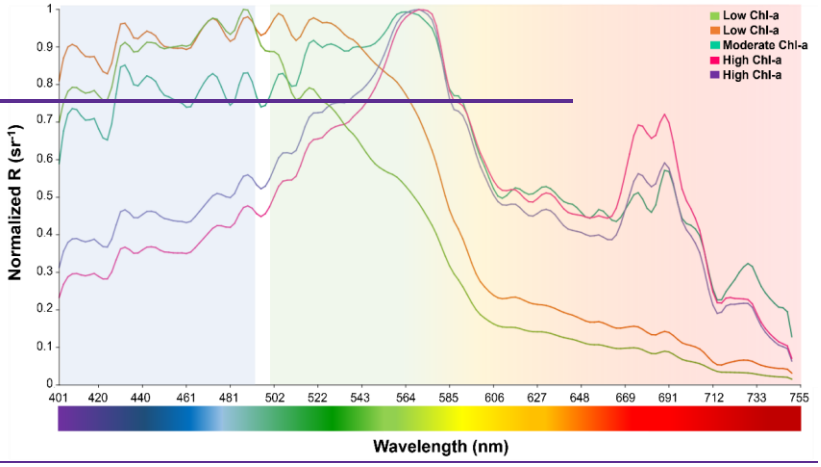

Figure 211: Microphytoplankton spectral signals at different Chlorophyll-a concentration. Low chlorophyll-a (< 2 µg L^{-1}) (jasmine, green and orange lines); Moderate chlorophyll-a (> 4 to 7.9 µg L^{-1}) (aqua green line); and High chlorophyll-a (> 8 µg L^{-1}) (pink and purple lines).

Lastly, considering only the chlorophyll-a, the reflectance spectra displayed variability under different Chl-a concentrations (Fig. 9). Significant differences ($p < 0.01$) in spectra signals were detected at Ilque, with *Rhizosolenia* dominant, between January (low Chl-a= 0.8 µg L^{-1}) and March (high Chl-a= 1.6 µg L^{-1}). Also, in January, Pulelo (low Chl-a= 2.92 µg L^{-1}) and Isla Tenglo (high Chl-a= 5.93 µg L^{-1}) exhibited significant differences ($p < 0.01$) with a *Pseudo-nitzschia* dominant. Regardless of the dominant species, at low Chl-a concentrations (< 2 µg L^{-1}), reflectance spectral signals exhibited more significant variability in the green-red bands (from 500 to 750 nm) bands, while under moderate (> 4 µg L^{-1}) to high (> 8 µg L^{-1}) Chl-a concentrations this variability was greater in the blue bands (~ 400-490 nm) bands (Fig. 911).

Con formato: Fuente: 10 pto, Sin Negrita

4 Discussion

4.1 Phytoplankton assemblages and spectral R(λ) variability

In the present work, we have obtained a hyperspectral R(λ) data set with a total of 20 R(λ) spectra which characterise the fingerprint of main phytoplankton groups and even the predominant genera in the northern Patagonia fjords (Iriarte et al., 2007; Alves-de-Souza et al., 2008; Jacob et al., 2014; Cuevas et al., 2019). These spectral fingerprints are representative of most dominant species-genera in the phytoplankton community composition and appear consistent even under varying oceanographic conditions. Our results are particularly relevant in a context where few datasets or studies include in situ hyperspectral reflectance (R(λ)) as a new approach for studying phytoplankton composition (Casey et al., 2020).

~~Currently, there are few datasets or studies that include in situ hyperspectral reflectance (R(λ)) as a new approach for studying phytoplankton composition (Casey et al., 2020). Through this study, a hyperspectral R(λ) data set, under variable oceanographic conditions, was created with a total of 20 R(λ) spectra, aiming to characterise the fingerprint of phytoplankton corresponding to the typical dominant species and total phytoplankton biomass concentrations in the study area (Iriarte et al., 2007; Alves-de-Souza et al., 2008; Jacob et al., 2014; Cuevas et al., 2019) under non-bloom conditions, except for the *Heterocapsa triquetra*.~~

~~The results reveal clear differences between the spectral signals of diatoms and dinoflagellates, in both shape and magnitude.~~ In our study, two main groups (diatoms and dinoflagellates) and three sub-groups of phytoplankton assemblages were identified through the R(λ) spectrum, exhibiting variability not only between groups but also among genera. Although the R(λ) spectrum from different diatom genera were quite similar in shape and magnitude across the blue to green bands (~ 400-520 nm), the spectral signal allowed us to distinguish the "fingerprints" of different genera. These differences are especially observed at the blue (~ 400-490 nm) and red to near infra-red bands (~ 650-740 nm), where the absorption and fluorescence of accessory pigments are highest (Kramer et al., 2022).

At the red to near infra-red bands (~ 650-740 nm) peaks of absorbance at 683 and 700 nm have been previously related to HAB (Shen et al., 2012) in concurrence with reflectance values drop registered for both diatoms and dinoflagellates groups in our~~this~~ study. Spectral studies have shown~~ed~~ differences in the signal of diatoms and dinoflagellates species (Tao et al., 2013). Zhao et al. 2010 described three different spectral fingerprints grouping several species. In that study, dinoflagellate *Heterosigma akashiwo* was characterized by a single reflectance peak at 680-750 nm. However, our results displayed a more accurate spectrum, due to the width of the spectral signal, with a doble peak structure between 670-690 nm, a plateau around 720-730 nm and a previous higher peak in the green bands at ~570 nm. This main peak has been previously described to characterize the HAB dinoflagellate species *Lepidodinium chlorophorum* spectral signal (Gernez et al., 2023), opening the possibility to be considered~~consider~~ as a dinoflagellates spectral signal characteristic. However, our hyperspectral reflectance results of diatoms species have showed a similar peak around 560-570 nm for *Skeletonema* sp., in coincidence with studies using satellite remote-sensing reflectance (Tao et al., 2013).

~~In our study, two main groups (diatoms and dinoflagellates) and three sub-groups of phytoplankton assemblages were identified through the R(λ) spectrum, exhibiting variability not only between groups but also among genera. Although the R(λ)~~

~~spectrum from different diatom genera were quite similar in shape and magnitude across the blue to green bands (~ 400-520 nm), the spectral signal allowed us to distinguish the "fingerprints" of different genera.~~

The pigments concentrations and the community composition of phytoplankton ~~and their~~ effects on the reflectance spectrum have been demonstrated to be essential factors in developing optical fingerprints at the genus or species levels (Mao et al., 2010; Kramer et al., 2022; Gernez et al., 2023). Although increases in absorbance and decreases in reflectance are generally correlated directly with changes in algal density (cell concentration) in monospecific laboratory experiments (Gitelson et al., 1999), non-significant differences in spectral signals under different cell concentrations was detected in our field monitoring. This lack of relationship between cell density and reflectance is probably seen in the range of densities observed in this study, which varied from 1,582,600 to 3,400 cells L^{-1}. In this context, the main factor affecting reflectance signals with differences in the shape of the curve for the same species, was related to pigment concentration (Chl-a). In fact, significant differences in major spectral bands (blue, green and red) were observed based on this pigment concentration. In summer, under low Chl-a concentrations, peaks in reflectance in the green-red (~ 500-750 nm) bands, where chlorophyll pigment reflects light, showed significant variability in both shape and magnitude of R(λ), among genera and localities. While, spectral signals registered in autumn, under a more diverse community and higher Chl-a concentrations, displayed more variability in the blue (~ 400-490 nm) bands. However, as indicated by Mao et al. (2010) the variations in the blue bands (400-450 nm) are driven by the species composition under low Chl-a concentrations, in contrast to the green (500-550 nm) bands.

Recent studies have described a co-variation between pigments, both accessory and specific groups, and optical properties such as fluorescence, scattering or cellular grouping (Kramer et al., 2022). In our~~this~~ study, total Chl-a has been shown to play a key role in the spectra with the R(λ) signal classification. The hierarchical cluster analysis (HCA) groups ~~together assemblages corresponding to~~ the same phytoplankton assemblages~~groups~~ and genera ~~detected~~ even under variable oceanographic conditions (mainly salinity and Chl-a), putting together ~~gathering~~ localities~~locations~~ ~~under~~ with similar total biomass concentration (Chl-a) and phytoplankton community composition.

Localities with open water circulation, under different dominant diatoms genera, characterised by low total biomass concentrations (min. < 1 µg L^{-1}), higher salinity and the presence of dinoflagellates (*Gyrodinium* sp. A~~a~~nd others tecate dinoflagellates) were grouped closer (Yaotal, Ilque and Pulelo). ~~While~~On the other hand, stations with high Chl-a concentrations (min. >1 µg L^{-1}), located mainly in enclosed areas like Chaparano and Canal Tenglo, were part of another group. Further, it must be pointed out that locations with the lowest Chl-a concentrations also displayed the lowest mean values of abundance~~, making it difficult to establish the role of phytoplankton pigments and cell concentration (density), in the R(λ) signal registered~~.

~~Biological factors such as community composition and pigment concentrations have been demonstrated to be determining factors to consider when studying reflectance signals. Even when measuring just Chl-a as a pigment, significant differences in major spectral bands were observed based on this pigment concentration. In summer, under low Chl-a concentrations, peaks in reflectance in the green-red bands (~ 500-750 nm) exhibited significant variability. While, spectral signals registered in~~

Con formato: Fuente: Sin Cursiva

Con formato: Fuente: Sin Cursiva

Con formato: Fuente: Sin Cursiva

Con formato: Fuente: Sin Cursiva

Con formato: Fuente: Sin Cursiva

Con formato: Fuente: Sin Cursiva

~~autumn, under a more diverse community and higher Chl-a concentrations, displayed more variability in the blue bands (~ 400-490 nm). However, as indicated by Mao et al. (2010) the variations in the blue bands (400-450 nm) are driven by the species composition under low Chl-a concentrations, in contrast to the green bands (500-550 nm).~~

~~In fsct~~fact, ~~t~~The variability in reflectance can be associated with many factors, from biological (community composition, cellular morphology, cell density, pigments composition and concentration or physiological status) to physical-chemical (suspended matter, stratification, the roughness of the surface or the specular reflection) and/or even meteorological (wind speed, solar radiation, cloudiness, or solar angle) (Gitelson et al., 1999; Kim et al., 2016; Muñoz et al., 2023). For instance, ~~It has to be considered that not only chlorophyll a interact with solar radiance, and therefore effecting absorbance/reflectance spectra, but also non-biological particles (CDOM & TSM) especially in coastal and estuarine optically complex waters (Mao et al., 2010; Flores et al., 2022; Muñoz et al., 2023).~~

~~S~~stratification plays a key role in vertical distribution of phytoplankton and matter at estuarine and coastal waters, ~~, where r~~River and glacier melting discharges constitute an important input of CDOM and TSM which alters the bio-optical signal, especially at blue bands (Simis et al., 2017; Kramer et al., 2022; Adhikari et al., 2023). In the Patagonian ~~F~~fjords, and especially within the Chiloé Inner Sea, high synchrony between Chl-a and turbid river plumes has been detected using remote sensing reflectance (Rrs_{645} product) at 645 nm (Muñoz et al., 2023).

In fact, variations in bio-optical water properties have been related not just to a punctual parameter but to their interactions and seasonality (Flores et al., 2022; Adhikari et al., 2023; Muñoz et al., 2023), with changes in the optical signal associated to both biological (phytoplankton succession) and non-biological (stratification) characteristics in the water column (Simis et al., 2017). Also, to distinguish the effect of different factors on in situ reflectance signals is quite complex since that could be a nonlinear relationship. Therefore, further research is necessary to understand both biological, i.e. phytoplankton composition and pigment concentration, including accessory pigments, and non-biological particles on the reflectance signal.

4.2 New technologies: limitations, opportunities and challenges

Optical technologies~~, like satellites,~~ for phytoplankton remote detection, like satellites, have been employed for decades (Hu et al., 2005; Shen et al., 2012; Moisan et al., 2017; Gernez et al., 2023). Although limitations in satellite observations associated with spatial-temporal and spectral bands resolution are well known (Muller-Karger et al., 2018; Schaeffer and Myer, 2020), recently new satellites using multi- or hyperspectral sensors like Plankton, Aerosol, Cloud, ocean Ecosystem (PACE) and Hyperspectral Imager for the Coastal Ocean (HICO) have shown improvements in spatial (~ 1200-90 m) and/or spectral resolution (~ 350-900 nm) (Kramer et al., 2022; Gernez et al., 2023) favouring the observation in the ultraviolet (UV), visible and near-infrared bands. However, limitations remain associated with the number of spectral bands and the satellite orbit cycle or caused by cloud cover and sun glint at remote areas.

Accurate observations represent a challenge in coastal areas where phytoplankton spatial-temporal variability changes rapidly. The recent development of new technologies, like UAV and hyperspectral cameras, to detect and monitor phytoplankton

Con formato: Fuente: Sin Cursiva

blooms, focusing on harmful algae species at a high spatial-temporal resolution, can fill in the gaps of satellite data and also be able to validate satellite data with in situ measurements.

The usefulness of this technology at in situ measurements has been demonstrated, especially in coastal areas with current or future economic activities (Kim et al., 2016; Kimura et al., 2019; McEliece et al., 2020; Min et al., 2021). Thus, an essential factor is the chosen optical system ~~chosen~~ for the spectral signal capture. Currently, there are multiple possibilities, i.e., radiometers, hyperspectral and multispectral cameras, which offer different characteristics such as spectral resolutions, sizes and imaging systems (Kislik et al., 2018; Olivetti et al., 2023). Although hyperspectral cameras represent a high-cost technology nowadays, the high resolution of these cameras is considered the best option for phytoplankton and HAB monitoring in complex and small coastal areas with aquaculture activities such as fjords, bays and estuaries (Olivetti et al., 2023).

Our~~This~~ study has identified a series of advantages and challenges ~~with~~ using UAV and hyperspectral technology for detecting and identifying phytoplankton assemblages in complex coastal waters. One of these ~~the first~~ advantages is the continuous spectral resolution that the~~a~~ hyperspectral camera provides, measuring each ~ 2 nm from 400 to 1000 nm ~~approx., in comparison to multisensor cameras and satellites available, being~~ which is a powerful tool for differentiating between phytoplankton assemblages through changes in spectral signals at high spectral resolution.

~~In our study area, a coastal system with a complex topography and high cloud cover throughout the year, capturing an effective satellite reflectance signal is a major challenge, especially on the same day and hour when water samples are being taken. Therefore, using a~~ The use of UAV for in situ reflectance measurement ~~when a bloom has been declared~~ is another advantage~~,~~. For instance, the~~with the possibility of~~ monitoring at optimal altitudes (< 100 m) allow a very high spatial resolution (~3.5 cm by pixel) and also to obtain reflectance under cloud cover or other atmospheric factors such as suspended dust and other particles. These advantages is contrasted with the major challenges for capturing satellite reflectance in a coastal system with a complex topography and high cloud cover throughout the year, especially if it is necessary to obtain images~~imagen~~ on the same day and hour when water samples are being taken. ~~Also, it must be mentioned that non high-qualified personnel are needed to drive the UAV.~~

However, the use of UAV as a platform for phytoplankton monitoring in remote areas is still a challenge. Although this technology could shorten sampling times and give us the possibility of monitor at local coastal remote areas, the dependency on a good network signal in the area constitutes a major limitation, particularly in remote areas where the network signal is easily lost. Also, weather conditions such as wind speed or rain ~~precipitation~~, as previously identified (Kislik et al., 2018), can compromise ~~the ability to fly, limiting~~ the use of a UAV ~~to monitor phytoplankton and HAB~~. Other limitations that appeared frequently during the study were related to technical aspects such as the flight time limited by the battery's life~~, the area coverage limited by the network signal and again batteries durability, or~~ and the lack of reference points in a continuous body water (Kislik et al., 2018; Wu et al., 2019). ~~The battery's life was identified as a quite important aspect being the main factor that spatially limited the monitoring to coastal areas and also few stations barely separated during the study.~~ Another aspect to

consider is the camera size. Nowadays hyperspectral cameras are still new being not yet completely functional due to their big size and weight that force to acquire a bigger drone and therefore a more expensive one. Related to the camera, one more aspect that can be a challenge is the high variability at cameras market with different characteristics in spectral resolution, geometry acquisition and imaging systems. ~~Although this can be considered at first as a positive point, we have to be~~ For instance, cautiousness should be taken at the moment to acquire the camera because this could ~~is going to~~ limit the possibility to compare data and apply algorithms in future.

Other important barriers which make it difficult to identify phytoplankton using reflectance data are the analysis of the vertical distribution of phytoplankton in the water column (~ 1-40 m) in both satellites and UAV-hyper~~e~~spectral camera systems, especially in the design of future algorithms. Therefore, not just the phytoplankton distribution in water column but also the presence of other particles, mainly non-biological ones, and their impact in solar radiation absorption/reflexion together with physical aspects as the water roughness.

~~Although recent works have been including hyperspectral data for the study of phytoplankton assemblages, these datasets are still limited to specific areas and unavailable, being the lack of a robust hyperspectral images' library another important factor to consider.~~

The high resolution of this new technology should allow us to improve the classical detection algorithms based on reflectance and/or absorbance ratios employed until now using satellite data (Mao et al., 2010; Tao et al., 2013; Gernez et al., 2023). However, although recent works have been including hyperspectral data for the study of phytoplankton assemblages, these datasets are still limited to specific areas and/or unavailable, being the lack of a robust hyperspectral images' library another important factor to consider. ~~The reflectance data registered in this study, together with information on oceanographic conditions and phytoplankton pigments and associated genera fingerprints, can be employed in a next step for the development of an accurate algorithm through machine learning not just to identify and differentiate phytoplankton genera blooms but also non-biological particles (suspended materials, sediments, etc.) and water characteristics.~~ Therefore, future observations must combine UAV-hyperspectral~~UAV hyperespectral~~ camera system and next generation satellite hyperspectral data with in situ biological (phytoplankton concentration, pigments, and taxonomy) and non-biological data (CDOM & TSM) collected at multiples and diverse environments.

5 Conclusions

This study aimed to take the first steps in identifying phytoplankton from in situ hyperspectral signals using UAV and hyperspectral technologies~~y~~ in a complex coastal system such as the Patagonian ~~F~~fjords. Our results show the potential of hyperspectral data for detection and identification of phytoplankton assemblages providing evidence of differences between the spectral signals of diatoms (e.g., *Rhizosolenia* sp., *Pseudo-nitzschia* sp., and *Leptocylindrus* sp.) detected in the blue band (~ 400-490 nm) with those of dinoflagellates (e.g., *Heterocapsa triquetra*) observed in the red to near-red bands (~ 650-740

nm), regardless cellular concentration. Additionally, pigment concentrations have been validated as determinants, with Chl-a playing a significant role in classifying the reflectance spectra signal. Our study illustrates the great potential of hyperspectral technology and the usefulness of UAV systems to support and improve both satellite and in situ monitoring in complex coastal waters ~~to advance ecological knowledge and environmental management. Thus, the hyperspectral sensor coupled to a UAV in remote areas could fill the satellite data gaps resulting from high cloud cover and extreme environmental conditions typical in the~~ such as Patagonian ~~F~~fjords. The reflectance data registered in this study, associated with specific genera label, together with information on oceanographic conditions and phytoplankton pigments, can be employed in a next step for the development of an accurate algorithm through machine learning not just to identify and differentiate phytoplankton genera blooms but also non-biological particles (suspended materials, sediments, etc.) and other water characteristics. ~~Finally, future analysis focusing on the impacts of varying water conditions and physical-chemical characteristics on the optical properties of the water and the reflectance spectrum (R(λ)) together with accessory cellular pigments need to be undertaken.~~

Con formato: Fuente: Sin Cursiva

6 Data Availability Statement

The datasets for this study can be found in the https://doi.org/10.5281/zenodo.16574287 or by request from the corresponding authors.

7 Author Contributions

Conceptualisation, PA and DV; methodology, PA and DP; validation, DV, IP and DP; formal analysis, PA and DP; investigation, PA, DP and CV; resources, DV; data curation, PA and DP; writing-original draft preparation, PA; writing-review and editing, DV, IP, DP, CV and PA; visualisation, PA and CV; supervision, DV; project administration, DV; funding acquisition, DV. All authors have read and agreed to the published version of the manuscript.

8 Competing interests

The authors declare that they have no conflict of interest.

9 Acknowledgements

We thank Ocean Data View, PRIMER and PAST software's for the data analysis and the construction of figures in the manuscript. Also, we thank Pamela Urrutia from MOWI, Cristobal Valdivieso and Lixandro Cisternas from ADENTU Ingeniería SpA, and Constanza Obando and Elson Stuard for UAV training, technical and adequacy, and Dr Mattew Lee for meticulous review of the manuscript.

10 Financial support

This research was funded by FONDEF ID20I10369 and ID24I10271.

References

Adhikari, A., Menon, H.B., and Lotliker, A.: Coupling of hydrography and bio-optical constituents in a shallow optically complex region using ten years of in-situ data, ISPRS J. Photogramm., 202, 499-511, https://doi.org/10.1016/j.isprsjprs.2023.07.014, 2023.

Alves-de-Souza, C., González, M.T., and Iriarte, J.L.: Functional groups in marine phytoplankton assemblages dominated by diatoms in fjords of southern Chile, J. Plankton Res., 30, 1233-1243, https://doi.org/10.1093/plankt/fbn079, 2008.

Anderson, D.: HABs in a changing world: a perspective on harmful algal blooms, their impacts, and research and management in a dynamic era of climactic and environmental change, Harmful Algae, 3:17, 2012.

Berdalet, E., Fleming, L.E., Gowen, R., Davidson, K., Hess, P., Backer, L.C., Moore, S.K., Hoagland, P., and Enevoldsen, H.: Marine harmful algal blooms, human health and wellbeing: challenges and opportunities in the 21st century, J. Mar. Biol. Assoc. U. K., 96(1), 61-91, https://doi.org/10.1017/S0025315415001733, 2016.

Casey, K.A., Rousseaux, C.S., Gregg, W.W., Boss, E., Chase, A.P., Craig, S.E., Mouw, C.B., Reynolds, R.A., Stramski, D., Ackleson, S.G., Bricaud, A., Schaeffer, B., Lewis, M.R., and Maritorena, S.: A global compilation of in situ aquatic high spectral resolution inherent and apparent optical property data for remote sensing applications, Earth Syst. Sci. Data, 12, 1123-1139, https://doi.org/10.5194/essd-12-1123-2020, 2020.

Castillo, M.I., Cifuentes, U., Pizarro, O., Djurfeldt, L., and Caceres, M.: Seasonal hydrography and surface outflow in a fjord with a Deep sill: the Reloncaví fjord, Chile, Ocean Sci., 12, 533-544, https://doi.org/10.5194/os-12-533-2016, 2016.

Clarke, K.R., and Gorley, R.N.: PRIMER v7: User Manual/Tutorial, PRIMER-E Plymouth, 2015.

Cuevas, L.A., Tapia, F.J., Iriarte, J.L., González, H.E., Silva, N., and Vargas, C.A.: Interplay between freshwater discharge and oceanic waters modulates phytoplankton size-structure in fjords and channel systems of the Chilean Patagonia, Prog. Oceanogr., 173, 103-113, https://doi.org/10.1016/j.pocean.2019.02.012, 2019.

Dávila, P.M., Figueroa, D., and Müller, E.: Freshwater input into the coastal ocean and its relation with the salinity distribution off austral Chile (35–55°S), Cont. Shelf Res., 22, 521-534, 2002.

Díaz, P.A., Álvarez, G., Varela, D., Pérez-Santos, I., Díaz, M., Molinet, C., Seguel, M., Aguilera-Belmonte, A., Guzman, L., Uribe, E., Rengel., J., Hernández, C., Segura, C., and Figueroa, R.I.: Impacts of harmful algal blooms on the aquaculture industry: Chile as a case study, Perspectives in Phycol., 6(1-2), 39-50, https://doi.org/10.1127/pip/2019/0081, 2019.

Flores, R.P., Lara, C., Saldías, G.S., Vásquez, S.I., and Roco, A.: Spatio-temporal variability of turbid freshwater plumes in the Inner Sea of Chiloé, northern Patagonia, J. Mar. Syst., 228, 103709, https://doi.org/10.1016/j.jmarsys.2022.103709, 2022.

Gallagher, N.B.: Savitzky-Golay smoothing and differentiation filter, Eigenvector Research Inc., www.eigenvector.com. https://doi.org/10.13140/RG.2.2.20339.50725, 2020.

Garreaud, R., Lopez, P., Minvielle, M., and Rojas, M.: Large-Scale Control on the Patagonian Climate, J. Clim., 26, 215-230, https://doi.org/10.1175/JCLI-D-12-00001.1, 2013.

Gernez, P., Zoffoli, M.L., Lacour, T., Hernández Fariñas, T., Navarro, G., Caballero, I., and Harmel, T.: The many shades of red tides: Sentinel-2 optical types of highly-concentrated harmful algal blooms, Remote Sens. Environ., 287, 113486, https://doi.org/10.1016/j.rse.2023.113486, 2023.

Gitelson, A.A., Schalles, J.F., Rundquist, D.C., Schiebe, F.R., and Yacobi, Y.Z.: Comparative reflectance properties of algal cultures with manipulated densities, J. Appl. Phycol., 11, 345-354, 1999.

Glibert, P.M.: Harmful algae at the complex nexus of eutrophication and climate change, Harmful Algae, 91, 101583, https://doi.org/10.1016/j.hal.2019.03.001, 2020.

Gobler, C.J.: Climate Change and Harmful Algal Blooms: Insights and perspective, Harmful Algae, 91, https://doi.org/10.1016/j.hal.2019.101731, 2020.

González, H.E., Nimptsch, J., Giesecke, R., and Silva, N.; Organic matter distribution, composition and its possible fate in the Chilean North-Patagonian estuarine system, Sci. Total Environ., 657, 1419-1431, https://doi.org/10.1016/j.scitotenv.2018.11.445, 2019.

Hallegraeff, G.M., Anderson, D.M., Belin, C., Dechraoui Bottein, M-Y., Bresnan, E., Chinain, M., Enevoldsen, H., Iwataki, M., Karlson, B., Mckenzie, C.H., Sunesen, I., Pitcher, G.C., Provoost, P., Richardson, A., Schweibold, L., Tester, P.A., Trainer, V.L., Yñiguez, A.T., and Zingone, A.: Perceived global increase in algal blooms is attributable to intensified monitoring and emerging bloom impacts, Commun. Earth Environ., 2, 117, https://doi.org/10.1038/s43247-021-00178-8, 2021.~~Hallegraeff et al., 2021~~

Hammer, Ø., Harper, D.A.T., and Ryan, P.D.: PAST: Paleontological Statistics Software Package for Education and Data Analysis, Palaeontologia Electronica, 4(1), 1-9, 2001.

Heisler, J., Glibert, P.M., Burkholder, J.M., Anderson, D.M., Cochlan, W., Dennison, W.C., Dortch, Q., Gobler, C.J., Heil, C.A., Humphries, E., Lewitus, A., Magnien, R., Marchall, H.G., Sellner, K., Stockwell, D.A., Stoecker, D.K., and Suddleson, M.: Eutrophication and harmful algal blooms: A scientific consensus, Harmful Algae, 8, 3-13, https://doi.org/10.1016/j.hal.2008.08.006, 2008.

Henson, S.A., Cael, B.B., Allen, S.R., and Dutkiewicz, S.: Future phytoplankton diversity in a changing climate, Nat. Commun., 12, 5372, https://doi.org/10.1038/s41467-021-25699-w, 2021.

Hong, S.M., Baek, S-S., Yun, D., Kwon, Y-H., Duan, H., Pyo J., and Cho K.H.: Monitoring the vertical distribution of HABs using hyperspectral imagery and deep learning models, Sci. Total Environ., 794, 148592, https://doi.org/10.1016/j.scitotenv.2021.148592, 2021.

Hu, C., Muller-Karger, F.E., Taylor, C.J., Carder, K.L., Kelble, C., Johns, E., and Heil, C.A.: Red tide detection and tracing using MODIS fluorescence data: A regional example in SW Florida coastal waters, Remote Sens. Environ., 97, 311-321, https://doi.org/10.1016/j.rse.2005.05.013, 2005.

Con formato: Color de fuente: Automático, Resaltar

Con formato: Color de fuente: Automático, Resaltar

673 IOC et al.: IOC, SCOR and IAPSO: The International Thermodynamic Equation of Seawater – 2010: Calculation and Use of
674 Thermodynamic Properties. Intergovernmental Oceanographic Commission, Manuals and Guides No. 56, UNESCO, 196 pp.,
675 2010.
676 Iriarte, J.L., González, H.E., Liu, K.K., Rivas, C., and Valenzuela, C.: Spatial and temporal variability of chlorophyll and
677 primary productivity in surface waters of southern Chile (41.5-43°S), Estuarine, Coastal Shelf Sci., 74, 471-480,
678 https://doi.org/10.1016/j.ecss.2007.05.015, 2007.
679 Jacob, B.G., Tapia, F.J., Daneri, G., Iriarte, J.L., Montero, P., Sobarzo, M., and Quiñones, R.A.: Springtime size-fractionated
680 primary production across hydrographic and PAR-light gradients in Chilean Patagonia (41–50°S), Prog. Oceanogr., 129, 75-
681 84, https://doi.org/10.1016/j.pocean.2014.08.003, 2014.
682 Jeffrey, S.W., and Vesk, M.: Introduction to marine phytoplankton and their pigment signatures, in: Phytoplankton Pigments
683 in Oceanography: Guidelines to Modern Methods, edited by: Jeffrey, S.W., Mantoura, R.F.C., and Wright, S.W., UNESCO
684 Publ., Paris, France, 37-84, 1997.
685 Kim, H.M., Yoon, H.J., Jang, S.W., Kwak, S.N., Sohn, B.Y., Kim, S.G., and Kim, D.H.: Application of Unmanned Aerial
686 Vehicle Imagery for Algal Bloom Monitoring in River Basin, Int. J. Control Autom., 9, 203-220, 2016.
687 Kimura, F., Morinaga, A., Fukushima, M., Ishiguro, T., Sato, Y., Sakaguchi, A., Kawashita, T., Yamamoto, I., and Kobayashi,
688 T.: Early Detection System of Harmful Algal Bloom Using Drones and Water Sample Image Recognition, Sens. Mater.,
689 31(12), 4155-4171, https://doi.org/10.18494/SAM.2019.2417, 2019.
690 Kislik, C., Dronova, I., and Kelly, M.: UAVs in Support of Algal Bloom Research: A Review of Current Applications and
691 Future Opportunities, Drones, 2:35, https://doi.org/10.3390/drones2040035, 2018.
692 Kramer, S.J., Siegel, D.A., Maritorena, S., and Catlett, D.: Modeling surface ocean phytoplankton pigments from hyperspectral
693 remote sensing reflectance on global scales, Remote Sens. Environ., 270-112879, https://doi.org/10.1016/j.rse.2021.112879,
694 2022.
695 Legendre, L.: The significance of microalgal blooms for fisheries and for the export of particulate organic carbon in oceans, J.
696 Plankton Res.,12(4),681-699, 1990.
697 León-Muñoz, J., Urbina, M.A., Garreaud, R., and Iriarte, J.L.: Hydroclimatic conditions trigger record harmful algal bloom in
698 western Patagonia (summer 2016), Nature Sci. Rep., 8, 1330, https://doi.org/10.1038/s41598-018-19461-4, 2018.
699 Le Quéré, C., Harrison, S.P., Prentice, C., Buitenhuis, E.T., Aumont, O., Bopp L., Claustre, H., Cotrim Da Cunha, L., Geider,
700 R., Giraud, X., Klaas, C., Kohfeld, K.E., Legendre, L., Manizza, M., Platt, T., Rivkin, R.B., Sathyendranath, S., Uitz, J.,
701 Watson, A.J., and Wolf-Gladrow, D.: Ecosystem dynamics based on plankton functional types for global ocean
702 biogeochemistry models, Global Change Biol., 11, 2016-2040, https://doi.org/10.1111/j.1365-2486.2005.01004.x, 2005.
703 Li, Y., Zhou, Q., Zhang, Y., Li, J., and Shi, K.: Research Trends in the Remote Sensing of Phytoplankton Blooms: Results
704 from Bibliometrics, Remote Sens., 13, 4414, https://doi.org/10.3390/rs13214414, 2021.
705 Lincoqueo, S.L.: Catálogo de microalgas marinas, nocivas para salmónidos. Archipiélago de Chiloé, Kimeltuán SpA., 2019.

706 Linford, P., Pérez-Santos, I., Montero, P., Díaz, P.A., Aracena, C., Pinilla, E., Barrera, F., Castillo, M., Alvera-Azcárate, A.,
707 Alvarado, M., Soto, G., Pujol, C., Schwerter, C., Arenas-Uribe, S., Navarro, P., Mancilla-Gutiérrez, G., Altamirano, R., San
708 Martín, J., and Soto-Riquelme, C.: Oceanographic processes driving low-oxygen conditions inside Patagonian fjords,
709 Biogeosciences, 21, 1433-1459, https://doi.org/10.5194/bg-21-1433-2024, 2024.
710 Mao, Z., Stuart, V., Pan, D., Chen, J., Gong, F., Huang, H., and Zhu, Q.: Effects of phytoplankton species composition on
711 absorption spectra and modelled hyperspectral reflectance, Ecol. Inform., 5, 359-366,
712 https://doi.org/10.1016/j.ecoinf.2010.04.004, 2010.
713 Mardones, J.I., and Clément, A.: Manual de microalgas del sur de Chile, Plancton Andino SpA., Puerto Varas, 186 pp., 2016.
714 McEliece, R., Hinz, S., Guarini, J.M., and Coston-Guarini, J.: Evaluation of Nearshore and Offshore Water Quality Assessment
715 Using UAV Multispectral Imagery, Remote Sens., 12, 2258, https://doi.org/10.3390/rs12142258, 2020.
716 Merkens, J.L., Reimann, L., Hinkel, J., and Vafeidis, A.T.: Gridded population projections for the coastal zone under the
717 Shared Socioeconomic Pathways, Glob. Planet. Change., 145, 57-66, https://doi.org/10.1016/j.gloplacha.2016.08.009, 2016.
718 Min, J.E., Lee, S.K., and Ryu, J.H.: Advanced surface-reflected radiance correction for airborne hyperspectral imagery in
719 coastal red tide detection, ISPRS Ann. Photogramm. Remote Sens. Spatial Inf. Sci., 3, 73-80, https://doi.org/10.5194/isprs-
720 annals-V-3-2021-73-2021, 2021.
721 Moisan, T.A., Rufty, K.M., Moisan, J.R., and Linkswiler, M.A.: Satellite Observations of Phytoplankton Functional Type
722 Spatial Distributions, Phenology, Diversity, and Ecotones, Front. Mar. Sci., 4, 189, https://doi.org/10.3389/fmars.2017.00189,
723 2017.
724 Moses, W.J., Gitelson, A.A., Perk, R.L., Gurlin, D., Rundquist, D.C., Leavitt, B.C., Barrow, T.M., and Brakhage, P.:
725 Estimation of chlorophyll-a concentration in turbid productive waters using airborne hyperspectral data, Water Res., 46, 993-
726 1004, https://doi.org/10.1016/j.watres.2011.11.068, 2012.
727 Muller-Karger, F.E., Hestir, E., Ade, C., Turpie, K., Roberts, D.A., Siegel, D., Miller, R.J., Humm, D., Izenberg, N., Keller,
728 M., Morgan, F., Frouin, R., Dekker, A.G., Gardner, R., Goodman, J., Schaeffer, B., Franz, B.A., Pahlevan, N., Mannino, A.G.,
729 Concha, J.A., Ackleson, S.G., Cavanaugh, K.C., Romanou, A., Tzortziou, M., Boss, E.S., Pavlick, R., Freeman, A., Rousseaux,
730 c.S., Dunne, J., Long, M.C., Klein, E., McKinley, G.A., Goes, J., Letelier, R., Kavanaugh, M., Roffer, M., bracher, A., Arrigo,
731 K.R., Dierssen, H., Zhang, X., Davis, F.W., Best, B., Guralnick, R., Moisan, J., Sosik, H.M., Kudela, R., Mouw, C.B., Barnard,
732 A.H., Palacios, S., Roesler, C., Drakou, E.G., Appeltans, W., and Jetz, W.: Satellite sensor requirements for monitoring
733 essential biodiversity variables of coastal ecosystems, Ecol. Appl., 28(3), 749-760, https://doi.org/10.1002/eap.1682, 2018.
734 Muñoz, R., Lara, C., Arteaga, J., Vásquez, S.I., Saldías, G.S., Flores, R.P., He, J., Broitman, B.R., and Cazelles, B.: Temporal
735 Synchrony in Satellite-Derived Ocean Parameters in the Inner Sea of Chiloé, Northern Patagonia, Chile, Remote Sens., 15,
736 2182, https://doi.org/10.3390/rs15082182, 2023.

737 Neumann, B., Vafeidis, A.T., Zimmermann, J., and Nicholls, R.J.: Future Coastal Population Growth and Exposure to Sea-
738 Level Rise and Coastal Flooding - A Global Assessment, PLoS ONE, 10(3):e0118571,
739 https://doi.org/10.1371/journal.pone.0118571, 2015.
740 Olivetti, D., Cicerelli, R., Martinez, J-M., Almeida, T., Casari, R., Borges, H., and Roig, H.: Comparing Unmanned Aerial
741 Multispectral and Hyperspectral Imagery for Harmful Algal Bloom Monitoring in Artificial Ponds Used for Fish Farming,
742 Drones, 7:410, https://doi.org/10.3390/drones7070410, 2023.
743 Pérez-Santos, I., Garcés-Vargas, J., Schneider, W., Ross, L., Parra, S., and Valle-Levinson, A.: Double-diffusive layering and
744 mixing in Patagonian fjords, Prog. Oceanogr., 129, 35-49, https://doi.org/10.1016/j.pocean.2014.03.012, 2014.
745 Ruffin, C., and King, R.L.: The analysis of hyperspectral data using Savitzky-Golay filtering-theoretical basis, IEEE
746 International Geoscience and Remote Sensing Symposium 1999 (IGARSS'99), 2, 756-758,
747 https://doi.org/10.1109/IGARSS.1999.774430, 1999.
748 Saldías, G.S., Sobarzo, M., and Quiñones, R.: Freshwater structure and its seasonal variability off western Patagonia, Prog.
749 Oceanogr., 174, 143-153, https://doi.org/10.1016/j.pocean.2018.10.014, 2019.
750 Schaeffer, B.A., and Myer, M.H.: Resolvable estuaries for satellite derived water quality within the continental United States,
751 Remote Sens. Lett., 11(6), 535-544, https://doi.org/10.1080/2150704X.2020.1717013, 2020.
752 Schlitzer, R.: Ocean Data View 2023, https://odv.awi.de.
753 Shen, Li., Xu, H., and Guo, X.: Satellite Remote Sensing of Harmful Algal Blooms (HABs) and a Potential Synthesized
754 Framework, Sensors, 12, 7778-7803, https://doi.org/10.3390/s120607778, 2012.
755 Shi, K., Zhang, Y., Qin, B., and Zhou, B.: Remote sensing of cyanobacterial blooms in inland waters: present knowledge and
756 future challenges, Sci. Bull., 64, 1540-1556, https://doi.org/10.1016/j.scib.2019.07.002, 2019.
757 Silva, N., Vargas, C.A., and Prego, R.: Land-ocean distribution of allochthonous organic matter in surface sediments of the
758 Chiloé and Aysén interior seas (Chilean Northern Patagonia), Cont. Shelf Res., 31, 330-339,
759 https://doi.org/10.1016/j.csr.2010.09.009, 2011.
760 Silva, N., and Vargas, C.A.: Hypoxia in Chilean Patagonian Fjords, Prog. Oceanogr., 129, 62-74,
761 https://doi.org/10.1016/j.pocean.2014.05.016, 2014.
762 Simis, S.G.H., Ylöstalo, P., Kallio, K.Y., Spilling, K., and Kutser, T.: Contrasting seasonality in optical biogeochemical
763 properties of the Baltic Sea, PLoS ONE, 12(4):e0173357, https://doi.org/10.1371/journal.pone.0173357, 2017.
764 Soto, D., León-Muñoz, J., Dresdner, J., Luengo, C., Tapia, F.J., and Garreaud, R.: Salmon farming vulnerability to climate
765 change in southern Chile: understanding the biophysical, socioeconomic and governance links, Rev Aquac., 11, 354-374,
766 https://doi.org/10.1111/raq.12336, 2019.
767 Soto, D., León-Muñoz, J., Garreaud, R., Quiñones, R.A., and Morey, F.: Scientific warnings could help to reduce farmed
768 salmon mortality due to harmful algal blooms, Mar. Policy., 132, 104705, https://doi.org/10.1016/j.marpol.2021.104705, 2021.

~~Sournia, A.: Red-tide and toxic marine phytoplankton of the world ocean: an inquiry into biodiversity, in: Harmful marine algal blooms: Proceedings of the Sixth International Conference on toxic marine phytoplankton, edited by: Lassus P., et al., Lavoisier, France, 103-112, 1995.~~

Szekielda, K.H., Marmorino, G.O., Maness, S.J., Donato, T., Bowles, J.H., Miller, W.D., and Rhea, W.J.: Airborne hyperspectral imaging of cyanobacteria accumulations in the Potomac River, J. Appl. Remote Sens., 1, 013544, https://doi.org/10.1117/1.2813574, 2007.

Tao, B., Mao, Z., Pan, D., Shen, Y., Zhu, Q., and Chen, J.: Influence of bio-optical parameter variability on the reflectance peak position in the red band of algal bloom waters, Ecol. Inform., 16, 17-24, https://doi.org/10.1016/j.ecoinf.2013.04.005, 2013.

Torres, R., Silva, N., Reid, R., and Frangopulos, M.: Silicic acid enrichment of subantarctic surface water from continental inputs along the Patagonian archipelago interior sea (41–56°S), Prog. Oceanogr., 129, 50-61, https://doi.org/10.1016/j.pocean.2014.09.008, 2014.

Trainer, V.L., Moore, S.K., Hallegraeff, G., Kudela, R.M., Clement, A., Mardones, J.I., and Cochlan, W.P.: Pelagic harmful algal blooms and climate change: Lessons from nature's experiments with extremes, Harmful Algae, 91, 101591, https://doi.org/10.1016/j.hal.2019.03.009, 2020.

Troupin, C., Barth, A., Sirjacobs, D., Ouberdous, M., Brankart, J-M., Brasseur, P., Rixen, M., Alvera-Azcárate, A., Belounis, M., Capet, A., Lenartz, F., and Toussaint, M-E.: Generation of analysis and consistent error fields using the Data Interpolating Variational Analysis (Diva), Ocean Modelling, 52-53, 90-101, https://doi.org/10.1016/j.ocemod.2012.05.002, 2012.

Ugarte, A., Romero, J., Farías, L., Sapiains, R., Aparicio-Rizzo, P., Ramajo, L., Aguirre, C., Masotti, I., Jacques, M., Aldunce, P., Alonso, C., Azócar, G., Bada, R., Barrera, F., Billi, M., Boisier, J., Carbonell, P., De la Maza, L., De la Torre, M., Espinoza-González, O., Faúndez, J., Garreaud, R., Guevara, G., González, M., Guzmán, L., Ibáñez, J., Ibarra, C., Marín, A., Mitchell, R., Moraga, P., Narváez, D., O'Ryan, R., Pérez, C., Pilgrin, A., Pinilla, E., Rondanelli, R., Salinas, M., Sánchez, R., Sanzana, K., Segura, C., Valdebenito, P., Valenzuela, D., Vásquez, S., and Williamson, C.: «Marea roja» y cambio global: elementos para la construcción de una gobernanza integrada de las Floraciones de Algas Nocivas (FAN), Centro de Ciencia del Clima y la Resiliencia (CR)2, (ANID/FONDAP/15110009), 1-84, available on www.cr2.cl/fan, 2022.

Utermöhl, H.: Zur Vervollkommung der quantitativen Phytoplankton-Methodik. Mitteilungen Internationale Vereinigung für Theoretische und Angewandte Limnologie, 9, 1-38, 1985.

Valle-Levinson. A.: Contemporary Issues in Estuarine Physics, Cambridge University Press, New York, USA, 273-307, 2010.

Van der Merwe, D., and Price, K.P.: Harmful Algal Bloom Characterization at Ultra-High Spatial and Temporal Resolution Using Small Unmanned Aircraft Systems, Toxins, 7, 1065-1078, https://doi.org/10.3390/toxins7041065, 2015.

Wu, D., Li, R., Zhang, F., and Liu, J.: A review on drone-based harmful algae blooms monitoring, Environ Monit. Assess., 191-211, https://doi.org/10.1007/s10661-019-7365-8, 2019.

Xie, H., Luo, X., Xu, X., Tong, X., Jin, Y., Pan, H., and Zhou, B.: New hyperspectral difference water index for the extraction of urban water bodies by the use of airborne hyperspectral images, J. Appl. Remote Sens., 8(1), 085098-085098, https://doi.org/10.1117/1.JRS.8.085098, 2014.

Zhao, D.Z., Xing, X.G., Liu, Y.G., Yang, J.H., and Wang, L.: The relationship of chlorophyll-a concentration with the reflectance peak near 700 nm in algae-dominated waters and sensitivity of fluorescence algorithms for detecting algal bloom, Int. J. Remote Sens., 31, 39-48, https://doi.org/10.1080/01431160902882512, 2010.